cGAS activation converges with intracellular acidification to promote STING aggregation and pyroptosis in tumor models

Authors: Li Xiao[#,1], Yuan-li Ai[#,1], Xiang-yu Mi[#,1], Han Liang[#,2], Xiang Zhi[#,1], Liu-zheng Wu[1], Qi-tao Chen[1], Tong Gou[2], Chao Chen[2], Bo Zhou[1], Wen-bin Hong[1], Lu-ming Yao[1], Jun-jie Chen[2], Xianming Deng*[,1], Fu-nan Li*[,2], Qiao Wu*[,1], Hang-zi Chen*[,1]

Affiliations:

[1] State Key Laboratory of Cellular Stress Biology, The First Affiliated Hospital of Xiamen University, School of Life Sciences, Xiamen University, Xiamen, Fujian 361102, China.

[2] Fujian Provincial Key Laboratory of Innovative Drug Target Research, School of Pharmaceutical Sciences, Xiamen University, Xiamen 361102, China.

[#]These authors contributed equally to this work.

*Corresponding author.

Address correspondence to: Hang-zi Chen, Qiao Wu or Xianming Deng, School of Life Sciences, Xiamen University, 4221-120 South Xiang 'an Road, Xiamen, Fujian 361102, China. Phone:86-592-2181601; Email: chenhz@xmu.edu.cn (H.Z.C.); qiaow@xmu.edu.cn (Q.W.); xmdeng@xmu.edu.cn (X.M.D.). Or to: Fu-nan Li, School of Pharmaceutical Sciences, Xiamen University, 4221-115 Xiang 'an South Road, Xiamen, Fujian 361102, China. Phone: 86-592-2182453 ; Email: fnlee@xmu.edu.cn (F.N.L.).

Competing Financial Interests statement:

All authors disclosed no relevant relationships.

One Sentence Summary: cGAS-STING signaling triggers pyroptosiss

Key words: STING; cGAS; PERK; GSDME; Pyroptosis

Abstract

The cyclic GMP-AMP synthase (cGAS)-stimulator of interferon genes (STING) pathway is intimately associated with anti-tumoral immunity; however, the direct involvement of this pathway in tumor cell demise remains elusive. Here, we identified a compound dodecyl 6-hydroxy-2-naphthoate (DHN) that induces pyroptosis in melanoma cells through activating the non-canonical cGAS-STING signaling. DHN targets mitochondrial protein cyclophilin D (CypD) to induce the release of mitochondrial DNA, leading to cGAS activation and cyclic GMP-AMP (cGAMP) generation. Meanwhile, DHN-caused intracellular acidification induces PRKR-like endoplasmic reticulum kinase (PERK) activation, which promotes STING phosphorylation and polymerization in the presence of cGAMP, thereby facilitating the aggregation of STING in the endoplasmic reticulum, which serves as a platform to recruit Fas associated via death domain (FADD) and caspase-8, leading to caspase-8 activation and subsequent gasdermin E (GSDME) cleavage, which ultimately results in pyroptosis of tumor cells and tumor regression in mouse models. The occurrence of this non-canonical cGAS-STING pathway-associated pyroptosis is also observed when both cGAS is activated and intracellular pH declines. Collectively, our findings reveal a pathway that links non-canonical cGAS-STING signaling to GSDME-mediated pyroptosis, thereby offering valuable insights for tumor therapy.

Introduction

Pyroptosis, a recently discovered form of regulated cell death, is mediated by members of the gasdermin family that undergo cleavage to generate the N-terminal domain responsible for cell membrane perforation(1). Several proteases have been identified for gasdermin cleavage, with caspases being prominent examples. For instance, activation of caspase-8 by metabolite α-ketoglutarate (α-KG) or tumor necrosis factor α (TNFα) leads to GSDMC cleavage and subsequent induction of pyroptosis in tumor cells(2, 3). Caspase-1/4/5/11 are known to cleave GSDMD during Gram-negative bacterial infections in many cases(4, 5). However, upon *Yersinia* infection, caspase-8 is implicated in GSDMD cleavage. In many literatures, caspase-3 has been reported to cleave GSDME following stimulation with chemotherapy drug(6-8), while co-culture with killer lymphocytes induces granzyme B-dependent GSDME cleavage(9). These studies underscore the significance of elucidating additional regulatory mechanisms governing protease-mediated gasdermin cleavage under different circumstances.

As a cytoplasmic DNA sensor, cGAS recognizes not only foreign microbial (viral and bacterial) DNA in the cytoplasm but also its own DNA. Upon activation by cytosolic DNA, cGAS catalyzes ATP and GTP to generate cGAMP, which binds to and activates STING. Activated-STING translocates from the endoplasmic reticulum (ER) to the Golgi apparatus where it undergoes polymerization. The polymerized STING recruits TBK1 to cause its auto-activation, thereby facilitating IRF3 phosphorylation. Phosphorylated-IRF3 then translocases into the nucleus to initiate interferon transcriptional expression(10). In tumor cells, cytoplasmic DNA accumulation arises due to defects in the DNA-damage response, chromosomal instability, replicative stress, reactivation of endogenous retroelements, or release of mitochondrial DNA. These events activate cGAS-STING signaling pathway leading to upregulation of type I IFNs proinflammatory cytokines and chemokines(11), thereby playing a crucial role in anti-tumor immunity.

In addition to its canonical pro-inflammatory effect, STING is also involved in the induction of regulatory cell death through a non-canonical pathway. Upon activation, STING localizes to the lysosome and triggers membrane permeabilization, leading to lysosomal cell death (LCD) in human myeloid cells(12). In neuronal cells, glutamate excitotoxicity activates STING, resulting in autophagic degradation of glutathione peroxidase 4 (GPX4), which is essential for neuronal redox homeostasis and thereby inducing ferroptosis(13). STING activation has been reported to mediate PANoptosis in diffuse large B-cell lymphoma (DLBCL) cells(14). However, the role of STING in pyroptosis remains controversial. On one hand, oxidative stress-induced cGAS-STING activation stimulates NLRP3 inflammasome-mediated pyroptosis in human nucleus pulposus cells(15); on the other hand, depletion of STING in renal cell carcinoma leads to caspase-8 activation and GSDMD-mediated pyroptosis(16). Yet, the interplay between cGAS-STING signaling and GSDME-dependent pyroptosis has not been elucidated.

PERK is a key sensor of the unfolded protein response (UPR) in the ER. Upon activation, PERK inhibits protein synthesis, maintains cellular oxidative homeostasis, and enhances ER quality control(17). Recently, the identification of a non-canonical cGAS-STING-PERK pathway has emerged as pivotal in regulating senescence and organ fibrosis through modulation of the translational program(18). However, whether PERK participates in pyroptosis induction through regulation of the cGAS-STING pathway remains unknown. Herein, we elucidate a mechanism whereby pyroptosis is induced by the non-canonical STING signaling regulated by PERK. A small molecule compound dodecyl 6-hydroxy-2-naphthoate (DHN) from our in-house library is identified to have a capability of binding to mitochondrial protein CypD, leading to mPTP opening and subsequent release of mtDNA to the cytoplasm. This process activates cGAS and results in cGAMP production. Additionally, DHN-induced intracellular acidification activates PERK that interacts with and phosphorylates STING upon

presence of cGAMP. This STING phosphorylation promotes its oligomerization, and subsequent aggregation in the ER, thereby providing a platform for recruitment and cleavage of GSDME by caspase-8, ultimately inducing pyroptosis. Overall, this study reveals the function and mechanism involved in the formation of STING-dependent aggregates for pyroptotic induction.

Results

Compound DHN induces pyroptosis through caspase-8 mediated GSDME cleavage

Considering the inherent resistance of melanoma cells to apoptosis, lytic cell death may offer a more effective therapeutic approach by activating anti-tumoral immunity. To identify agents capable of inducing lytic cell death, we screened our in-house compound library using the lactate dehydrogenase (LDH) release assay, a well-established method for quantifying lytic cell death. This proprietary library was collaboratively developed by our research team and partners, and primarily consists of derivatives of Csn-B and THPN, compounds known to induce apoptosis and autophagic cell death, respectively(19, 20). Our results demonstrated that a compound named DHN (dodecyl 6-hydroxy-2-naphthoate) is the most potent compound for inducing lytic cell death in A375 melanoma cells (Fig. 1A). Further morphological assessment following DHN treatment revealed characteristic pyroptotic features, including cell swelling and the formation of large bubbles from the plasma membrane, as indicated by red arrowheads in Figure 1B. This DHN-induced characteristic pyroptotic morphology was closely associated with LDH release, and cleavage of the pyroptotic executor GSDME in melanoma A375 cells as well as other cancer cell lines (Fig. 1B & S1A). Knockdown of GSDME, but not other gasdermin proteins, in A375 cells attenuated DHN-induced pyroptosis (Fig. 1C & S1B-S1C), demonstrating the involvement of GSDME-mediated pyroptosis. Notably, no DNA laddering or Annexin V^+/PI^- cells, which are typical apoptotic markers, were observed upon DHN

stimulation (Fig. S1D). Furthermore, pretreatment with Lip-1, Fer-1 (ferroptosis inhibitors), NSA, Nec-1 (necroptosis inhibitors), or TTM (a cuproptosis inhibitor) did not affect DHN-induced LDH release or pyroptotic morphology (Fig. S1E). Additionally, we investigated whether DHN could induce pyroptosis in non-tumor cells and found that DHN exhibits a diminished capacity for pyroptotic induction in non-tumor cells, including HK-2 human kidney proximal tubule epithelial cells, AC16 human cardiomyocytes, HEK293T human embryonic kidney cells, THP-1 human leukemia monocytic cells, HL-1 mouse cardiomyocytes, L929 mouse fibroblasts, primary mouse bone marrow-derived macrophages (BMDM) and bone marrow-derived dendritic cells (BMDC), as compared to A375 melanoma cells (Fig. S1F). Collectively, these findings indicate that DHN predominantly induces GSDME-dependent pyroptosis rather than apoptosis, ferroptosis, necroptosis, or cuproptosis in tumor cells.

Co-treatment with Z-VAD, a pan-caspase inhibitor, abrogated DHN-induced pyroptosis (Fig. 1D), suggesting the participation of a caspase protein in GSDME cleavage. In accordance with previous reports, incubation of immunoprecipitated GSDME protein with recombinant caspase-3 resulted in clear cleavage of GSDME in the *in vitro* assay(6, 7). However, we unexpectedly found that knockdown of caspase-3 in cells had no impact on DHN-induced pyroptosis (Fig. S1G), excluding the possibility of caspase-3-mediated GSDME cleavage upon stimulation with DHN. The treatment with DHN was found to markedly induce caspase-8 activation while only minimally activating caspase-3 (Fig. S1H). Co-treatment with Z-IETD, a specific inhibitor of caspase-8, or knockdown of caspase-8 effectively attenuated DHN-induced pyroptosis in A375 cells (Fig. 1E-1F & S1B), suggesting the involvement of caspase-8 in cleaving GSDME for pyroptotic induction. Although recombinant caspase-8 exhibited mild cleavage of GSDME under normal *in vitro* conditions, the appearance of the cleaved band of GSDME migrating at approximately 30~35 kDa was markedly enhanced as the pH value

decreased to 6.5 in the *in vitro* cleavage buffer (Fig. S1I), implying that caspase-8 is capable of cleaving GSDME directly within an acidic environment.

Given that caspase-8 cleaves its substrate after an Asp residue(21), different Asp residues around the hinge region of GSDME were mutated into Ala. The *in vitro* results showed that $GSDME^{D270A}$ completely blocked caspase-8-mediated cleavage (Fig. S1J), suggesting that caspase-8 may target GSDME Asp270 for cleavage, similar to caspase-3(6, 7). When different GSDME mutants were separately expressed in the GSDME knockdown A375 cells, only $GSDME^{D270A}$ completely blocked DHN-induced GSDME cleavage (Fig. 1G), thereby attenuating pyroptotic induction (Fig. 1H). Together, it is demonstrated that DHN serves as a compound capable of inducing pyroptosis through caspase-8-mediated cleavage of GSDME.

DHN targets mitochondrial protein CypD to promote the opening of mPTP

Subsequently, we aimed to elucidate the target of DHN. To achieve this, we synthesized a photoactive DHN probe (referred to DHN-P) that exhibited similar properties to DHN in inducing pyroptosis (Fig. S2A). We firstly detected the subcellular localization of DHN-P using click chemistry (Fig. 2A), and found that DHN-P predominantly colocalized with Tom20, a mitochondrial marker protein, while minimal colocalization was observed with CALR (an endoplasmic reticulum marker), GM130 (a Golgi apparatus marker), or LAMP2 (a lysosomal marker) (Fig. 2B), indicating that mitochondria may be the organelle for DHN function. Our previous studies have demonstrated that the induction of pyroptosis is associated with an upregulation of various reactive oxygen species (ROS)(2, 7, 8, 22). We thus investigated whether mitochondrial ROS (mito-ROS) are involved in DHN-induced pyroptosis. Treatment with DHN indeed resulted in a significant increase in mito-ROS levels, however, the scavenging of mito-ROS by mito-TEMPO or mitoQ, failed to rescue DHN-induced pyroptosis (Fig. S2B-C), which excludes the association between mito-ROS and DHN-induced pyroptosis.

To elucidate the crucial mitochondrial functions underlying DHN-induced pyroptosis, we employed various inhibitors and the results indicated that inhibition of electron transport chain by antimycin A, rotenone or oligomycin, suppression of TCA cycle by CPI-613 or DMN, and attenuation of fatty acid oxidation by ranolazine had no impact on DHN-induced pyroptosis. Furthermore, modulation of mitochondrial fission through Mdivi-1 treatment or regulation of mitochondrial calcium homeostasis via MCU-i4 did not affect DHN-induced pyroptosis either (Fig. S2C). However, cyclosporin A (CsA), an inhibitor targeting cyclophilin D (CypD) within the mitochondrial permeability transition pore (mPTP) complex, markedly blocked DHN-induced caspase-8 activation and GSDME-mediated pyroptotic cell death (Fig 2C). Similar results were also obtained in CypD knockdown cells (Fig 2D). Given that DHN-P could effectively pull down CypD, but not other components in mPTP complex such as Adenine nucleotide translocator1 (ANT1) and voltage dependent anion channel 1 (VDAC1), or proteins in ER (CALR) or Golgi apparatus (TGN46) (Fig. 2E), it is likely that DHN targets CypD for pyroptotic induction.

To further verify that CypD is the direct target of DHN, we conducted surface plasmon resonance (SPR) experiments and confirmed the direct interaction between DHN and CypD, with a dissociation constant (*Kd*) of 1.19 ± 0.068 μM (Fig. 2F). We additionally performed fluorescence labeling-based differential scanning fluorimetry (FL-DSF), a well-established method for evaluating protein-ligand interactions(23). The FL-DSF assay yielded a *Kd* value of 0.69 ± 0.33 μM (Fig. S2D). We also performed cellular thermal shift assays (CETSA) to detect drug-target interactions through analyzing melting temperature (Tm) shifts. Addition of DHN significantly enhanced the thermal stability of CypD (Fig. 2G), indicating direct binding of DHN to CypD. Molecular docking indicates the theoretical binding mode of DHN to CypD (PDB: 5CBV), in which the naphthalene ring of DHN forms a distinct cationic π-interaction with R97 of CypD, and Q105 forms a hydrogen bond with the oxygen atom while the

hydrophobic carbon chain of DHN lies flat in the pocket (Fig. S2E). When these two critical residues were mutated ($CypD^{R97A/Q105A}$), DHN could no longer bind to CypD (Fig. 2G). As a result, DHN failed to induce GSDME cleavage and pyroptosis in $CypD^{R97A/Q105A}$ expressing cells (Fig. 2H). Therefore, DHN induces pyroptosis through binding to CypD.

Considering the crucial role of CypD in mPTP(24), we propose that DHN may regulate mPTP opening by targeting CypD. Indeed, DHN augmented mPTP opening, which was effectively inhibited by either CypD knockdown or CsA treatment (Fig. 2I). The essential role of mPTP opening in DHN-induced pyroptosis is further supported by our observation that knockdown of ANT1, another constituent of the mPTP, also impaired DHN-induced mPTP opening, GSDME cleavage and subsequent pyroptosis (Fig. S2F-G). Together, these findings suggest that DHN binding to CypD facilitates mPTP opening, ultimately leading to pyroptosis.

DHN-induced mtDNA release activates the cytosolic cGAS

It has been reported that several NLRP3 inflammasome activators can induce the oxidation of mtDNA, resulting in the release of 500-650 bp fragments into the cytosol through mPTP- and VDAC-dependent channels (25). Upon DHN stimulation, we also observed a significant increase in the amount of mtDNA in the cytoplasmic fraction that was free from mitochondrial contamination (Fig. 3A & S3A). This release of mtDNA was effectively suppressed by treatment with CsA or knockdown of ANT1 or CypD (Fig. 3A & S3A), emphasizing the crucial role played by mPTP in DHN-induced mtDNA release. However, no obvious oxidation of mtDNA was detected upon DHN stimulation (Fig. S3B), and DNA fragments in the cytosolic samples within the range of 500-700 bp were barely observed via agarose gel electrophoresis (Fig. S3C). Moreover, while a ~600 bp mtDNA fragment in the cytosolic fraction was clearly detected by PCR following DHN treatment, PCR also successfully amplified a ~5000 bp mtDNA fragment (Fig. S3D), suggesting that DHN may

induce the release of mtDNA fragments exceeding 5000 bp in length. Given that only mtDNA fragments smaller than 700 bp can be released upon mPTP opening(26), it is unlikely that DHN induces direct mtDNA release from mitochondria via the mPTP channel. It has been documented that prolonged mPTP opening leads to mitochondrial rupture(27, 28). Indeed, DHN-induced mitochondrial rupture was clearly observed by transmission electron microscopy. Furthermore, the release of HSP60, a mitochondrial matrix protein, into the cytosol upon DHN stimulation confirmed mitochondrial rupture (Fig. S3E). The DHN-induced release of HSP60 and mtDNA could be effectively suppressed by CsA treatment or CypD knockdown (Fig. S3F-G). Therefore, it can be concluded that DHN may promote prolonged mPTP opening, leading to mitochondrial rupture and subsequent mtDNA release.

Consistent with previous report that cytoplasmic DNA triggers phase transition of cGAS to activate its activity(29), we did observe the formation of cGAS puncta in response to DHN stimulation (Fig. 3B, left), and this DHN-induced cGAS puncta formation could be abolished by treatment with 1,6-hexanediol (1,6-HD) (Fig. S3H), a small molecule known for melting phase-separated condensates, indicating the phase transition of cGAS upon DHN stimulation. Furthermore, CsA treatment or knockdown of CypD or ANT1 abrogated the formation of these DHN-induced cGAS puncta (Fig. 3B-C). The ability of DHN to induce cGAS puncta formation was lost when the interaction between CypD and DHN was disrupted by the R97A/Q105A mutation in CypD (Fig. S3I). These findings demonstrate a direct link between mPTP-mediated mtDNA release and activation of cGAS upon binding of DHN to CypD.

The activation of cGAS is crucial for DHN-induced pyroptosis, as evidenced by the effective attenuation of DHN-induced GSDME cleavage and pyroptosis through silencing cGAS expression or inhibiting cGAS activity using inhibitor G140(30) (Fig. 3D-E). Combined with the finding that neither knockdown of cGAS nor G140 treatment affected the DHN-induced mtDNA release (Fig. S3J), these experiments indicate that it is the release of mtDNA

that activates cGAS and induces pyroptosis. It is well-accepted that STING serves as a downstream effector of cGAS(10). Indeed, knockdown of STING markedly impaired DHN-induced GSDME cleavage and pyroptosis (Fig. 3F). However, DHN treatment failed to induce the phosphorylation of TBK1 and IRF3 (Fig. S3K), the downstream kinases in the classical cGAS-STING pathway(10), as well as regulate the transcription levels of classical downstream target genes associated with cGAS-STING signaling (including *CXCL10, IFNB, RSAD2, ISG15* and *RIG1*) (Fig. S3L). Moreover, inhibition of TBK1 by GSK8612(31) did not affect DHN-induced pyroptosis (Fig. S3M). Together, it appears that DHN may activate an alternative pathway within the cGAS-STING axis to induce pyroptosis

The aggregation of STING in the ER provides the platform for GSDME cleavage

We also discovered that DHN could induce the formation of punctate structures of STING in a manner dependent on cGAS activity (Fig. 4A) and mPTP opening (Fig. S4A-B). However, these STING puncta were not co-localized with cGAS (Fig. S4C), suggesting that the STING puncta are distinct from cGAS puncta. Knockdown of STING did not affect DHN-induced formation of cGAS puncta (Fig. S4D). Notably, these STING puncta were exclusively localized to the ER rather than the Golgi apparatus or mitochondria (Fig. 4B, S4E), resulting in obvious puncta appearance within ER in a cGAS- and STING-dependent manner (Fig. S4F). Transmission electron microscopy revealed condensed membranous structures resembling aggregates within the ER upon DHN stimulation (Fig. 4C), which could be abolished by cGAS inhibitor G140 (Fig. S4G) or knockdown of STING (Fig. S4H). Additionally, in cells expressing STING-APEX fusion protein, the APEX signal was prominently observed within these tangled ER structures upon DHN stimulation (Fig. 4D). Therefore, it is likely that DHN induces the aggregation of STING in the ER through activating cGAS.

It has been reported that phase separation of STING within the ER can prevent excessive activation of classical cGAS-STING signaling(32). However, treatment with 1,6-HD failed to disrupt DHN-induced punctate aggregates of STING (Fig. S4I), and expression of $STING^{EE/GG}$ mutants, known to abolish the STING phase-separator(32), had no effect on these aggregates either (Fig. S4J). These results suggest that the DHN-induced STING aggregate in the ER (termed ER-STING aggregate) is distinct from the STING phase-separator reported by other group(32), and may play a role in pyroptosis induction.

To investigate the function of these ER-STING aggregates in pyroptotic induction, we employed a detergent-free immunoprecipitation technique using an anti-HA antibody to selectively isolate ER-STING aggregates in HA-STING expressing A375 cells. The immunoprecipitants were found to contain the ER protein CALR, while Golgi protein GM130 and mitochondrial protein Tom20 were not detected (Fig. 4E), confirming the absence of contamination from the Golgi apparatus or mitochondria. Western blotting demonstrated the activated caspase-8, GSDME full-length (FL), and GSDME N-terminal (NT) within these ER-STING aggregates upon DHN stimulation (Fig. 4E). Confocal microscopy consistently indicated the co-localization of caspase-8 and GSDME with STING puncta in the presence of DHN (Fig. 4F). These results suggest the recruitment of caspase-8 and GSDME into the ER-STING aggregates. Since protein aggregates are typically resistant to mild detergents like Triton X-100, we fractionated these ER-STING aggregates into a Triton X-100-insoluble (TI) fraction. It was showed that DHN stimulation obviously increased STING levels in the TI fraction, in which active caspase-8, FL-GSDME and cleaved-GSDME were also detected (Fig. 4G). The FL-GSDME appeared to be more enriched in the TI fraction compared to the cleaved-GSDME, which is consistent with previous findings that upon cleavage, cleaved-GSDME tends to localize to the plasma membrane for pyroptosis execution(6). Knockdown of CypD, cGAS or STING, or inhibition of cGAS activity using G140 resulted in loss of active caspase-

8 and GSDME within the STING aggregates even in the presence of DHN (Fig. 4G, S4K). Proximity labeling assays also demonstrated that DHN enhanced proximity between STING and caspase-8/GSDME (Fig. 4H). Considering the role of STING as a scaffold protein(33), it is implicated that DHN-induced ER-STING aggregate represents a large protein complex, potentially serving as platforms to recruit and process the cleavage of GSDME by caspase-8 for pyroptosis induction. The underlying mechanism of caspase-8 activation within the ER-STING aggregates was further explored. Fas-associated death domain (FADD), an adaptor protein essential for death receptor-mediated caspase-8 activation(34), was investigated for its role in this process. Our results demonstrated that DHN stimulation substantially enhanced the interaction between STING and FADD (Fig. S4L, top). This STING-FADD interaction is essential for the recruitment of caspase 8 by STING in response to DHN stimulation, as knockdown of FADD completely abolished the interaction between STING and caspase-8, even in the presence of DHN (Fig. S4L, bottom). Consequently, no caspase-8 was detected in STING-dependent protein aggregates upon FADD knockdown. Furthermore, FADD knockdown also eliminated DHN-induced caspase-8 activation, GSDME cleavage, and pyroptosis (Fig. S4M). The DED domain plays a pivotal role in the mutual interaction between FADD and caspase-8. In FADD-knockdown cells, re-expression of wild-type FADD, but not $FADD^{\Delta DED}$, restored DHN-induced caspase-8 activation, GSDME cleavage, and pyroptosis (Fig. S4N). Similarly, in caspase-8-knockdown cells, re-expression of wild-type caspase-8, instead of $caspase\text{-}8^{\Delta DED}$, restored DHN-induced GSDME cleavage and pyroptosis (Fig. S4O). Collectively, these findings indicate that DHN-induced interaction of STING with FADD promotes the recruitment of caspase 8 into ER-STING aggregates, where caspase 8 is activated to cleave GSDME for pyroptosis execution.

Acid environment promotes the polymerization of STING for the formation of ER-STING aggregates

Since the formation of protein aggregates is typically resulted from protein polymerization(35), we investigated whether DHN-induced ER-STING aggregate is associated with the polymerization of STING. As anticipated, DHN markedly enhanced the formation of STING dimers and polymers, which could be abolished by knockdown of CypD and ANT1 (Fig. 5A, left & S5A) or inhibition of cGAS by G140 (Fig. 5A, right), indicating that the opening of mPTP and cGAS activity are essential for DHN-induced STING polymerization. Cys148 and Cys206 in STING play critical roles in the occurrence of STING polymers(36, 37). Mutation at Cys206 but not at Cys148 abrogated DHN-induced STING polymerization (Fig. 5B & S5B). Although C206S mutation did not influence STING dimerization, it impaired the formation of ER-STING aggregates (Fig. 5C), and subsequent pyroptotic cell death (Fig. S5C). It is likely that DHN-induced opening of mPTP and subsequent activation of cGAS facilitate the polymerization of STING, and this STING polymerization, rather than dimerization, leads to the formation of ER-STING aggregates.

cGAMP is the product of activated cGAS(38). Interestingly, incubation of cGAMP with A375 cells indued the dimerization of STING, in accordance with previous reports(36), however, it barely induced the polymerization of STING, the formation of ER-STING aggregates and pyroptosis (Fig. S5D-S5F), suggesting that cGAS activation alone is insufficient for STING polymerization, and other unknown factors may be involved in DHN-induced pyroptosis. Considering our finding that caspase-8 exhibited unique enhanced activity in an acidic environment to cleave GSDME (Fig. S1I), and DHN, a naphthol derivative, has weak acid property, we hypothesized that DHN might acidify the intracellular environment that benefits pyroptotic induction. Indeed, treatment with DHN, but not cGAMP, effectively induced dose-dependent acidification of the intracellular milieu (Fig. 5D, left & S5G). NH_4Cl

significantly rescued DHN-induced decline of intracellular pH (Fig. 5D, right), which was closely associated with a series of events, including inhibited STING polymerization (Fig. 5E), the suppression of ER-STING aggregates (Fig. 5F-5G), the decrease of caspase-8 activation and GSDME cleavage in TI fraction (Fig. 5H), and the inhibition of DHN-induced pyroptosis (Fig. 5I). Clearly, an acidic intracellular environment induced by DHN is a prerequisite for the formation of ER-STING aggregates and pyroptosis.

Considering the ER localization of the ER-STING aggregates, we speculated that pH level of the ER might be altered. For this end, we first developed a reliable method for assessing ER pH, wherein the double ratio variation in different pH values served as an indicator of the detection system (Fig. S5H). Utilizing this approach, it was demonstrated that DHN did acidify the ER environment in a dose-dependent manner and this acidification could be rescued by NH_4Cl treatment as expected (Fig. S5I), in accordance with the results observed in the cytoplasm. These findings align with previous knowledge that the ER lacks an intrinsic pH regulatory system and readily equilibrates its pH to cytoplasmic levels(39).

Since NH_4Cl failed to regulate DHN-induced cGAS puncta formation (Fig. S5J), and the decline in intracellular or ER pH caused by DHN remained unaffected by inhibition of CypD or STING (Fig. S5K-L), we postulated that cGAS activation and ER acidification are two independent pathways that synergistically contribute to the formation of ER-STING aggregates and subsequent pyroptosis. To further validate this hypothesis, we simulated cGAS activation with cGAMP or diABZI treatment, while inducing a decrease in intracellular and ER pH through lactic acid treatment (Fig. S5M), which is abundant in the tumor microenvironment and known to lower intracellular pH levels(40, 41). It was demonstrated that either cGAMP/diABZI treatment alone or lowering pH by lactic acid alone was insufficient to induce pyroptosis; however, simultaneous treatment with cGAMP/diABZI and lactic acid clearly induced GSDME cleavage and subsequent pyroptosis (Fig. 6A). Similar phenomena were also

observed upon co-treatment of HCl, but not sodium lactate, with cGAMP (Fig. S5N-O). Knockdown of LDHA/LDHB (which are essential for lactate metabolism) or AARS1/AARS2 (involved in protein lactylation) (34, 42) had no effect on pyroptosis induced by cGAMP plus lactic acid (Fig. S5P), thereby excluding the involvement of lactate metabolism or protein lactylation. Moreover, infection with HSV1, a DNA virus known to activate cGAS(43), could also trigger GSDME-mediated pyroptosis in the presence of lactic acid or HCl (Fig. 6B). In conclusion, when both cGAS activation and intracellular acidification are simultaneously achieved, the STING-dependent GSDME-mediated pyroptosis occurs.

PERK-induced STING phosphorylation facilitates the polymerization of STING

The mechanism by which an acidic environment facilitates STING polymerization and the formation of ER-STING aggregates remains unclear. We unexpectedly found that DHN induced a time-dependent phosphorylation of STING, as evidenced by the appearance of an upshifted band in a phostag gel, which could be abolished when cell lysates were incubated with CIAP (calf intestinal alkaline phosphatase) (Fig. 7A). Notably, treatment with NH_4Cl substantially impaired DHN-induced STING phosphorylation (Fig. 7A), demonstrating the association between intracellular acidity and STING phosphorylation. Considering the subcellular localization of STING in the ER, we employed various inhibitors, including GSK2656157 targeting PERK, GSK650394 targeting SGK1, GSK2850163 targeting IRE1α, LRRK2-IN-1 targeting LRRK2, sorafenib targeting FLT3, lenvatnib targeting KDR, and HG-9-91-01 targeting SIK to identify the specific ER-resident protein kinase involved in STING phosphorylation. Among these inhibitors, only GSK2656157 effectively impairs DHN-induced STING phosphorylation (Fig. 7B, top & S6A), implicating PERK as a crucial mediator of STING phosphorylation upon DHN stimulation. Knockdown of PERK inhibited DHN-induced STING phosphorylation (Fig. 7B, bottom, S6B). It has been reported that PERK can be

activated through autophosphorylation at the Thr982 residue(44). DHN treatment effectively enhanced PERK phosphorylation (Fig. 7C, top), and mutation of Thr982 or inhibition of PERK activity by GSK2656157 eliminated DHN-induced PEKR phosphorylation and the association of PERK with STING (Fig. 7C-D). Therefore, these findings suggested that DHN promotes autophosphorylation and activation of PERK, leading to the association of PERK with STING, and subsequent STING phosphorylation.

Recent studies have suggested that cGAS-STING activation directly triggers PERK activation(18). In contrast, inhibition of mtDNA release (CsA treatment or CypD knockdown) or suppression of cGAS-STING activity (G140 treatment or STING knockdown) did not affect PERK phosphorylation upon DHN stimulation (Fig. S6D), excluding the involvement of cGAS-STING in PERK activation during DHN treatment. Instead, NH_4Cl treatment profoundly suppressed DHN-induced PERK activation (Fig. 7E, top), and a decrease in intracellular pH caused by lactic acid, HCl or citric acid was sufficient to induce PERK phosphorylation and activation (Fig. 7E, bottom, S6E). Combined with the fact that inhibition of PERK by GSK2656157 or knockdown of PERK did not affect DHN-induced acidification (Fig. S6F), it could be concluded that PERK is activated when there is a decline in intracellular pH induced by DHN treatment.

Although inhibition of PERK did not affect cGAS puncta formation (Fig. S6G), it markedly impaired DHN-induced STING polymerization (but not dimerization), formation of ER-STING aggregates, cleavage of GSDME by caspase-8 within ER-STING aggregates, and subsequent pyroptosis (Fig. 7F-H; S6H-K), demonstrating the crucial role of PERK in STING polymerization but not in cGAS activation. According to PhosphoSitePlus database, there are four potential phosphorylated Ser/Thr residues in STING, including Thr84, Ser345, Ser358, and Ser366 (45, 46). Substituting alanine for either Ser345 or Ser358 weakly impaired DHN-induced STING phosphorylation (Fig. S6L), while combined mutation of these two residues

(STING$^{S345A/358A}$) resulted in the abrogation of DHN-induced STING phosphorylation in A375 cells (Fig. 8A, top) and PERK-induced STING phosphorylation *in vitro* (Fig. 8A, bottom), leading to the elimination in the polymerization of STING, formation of ER-STING aggregates, GSDME cleavage by caspase-8 in the TI fraction, and subsequent pyroptosis (Fig. 8B-D; S6M). Considering that the Cys206 mutation, which abolishes STING polymerization (Fig. 5B), had no impact on DHN-induced STING phosphorylation (Fig. S6N), it is plausible that PERK-mediated phosphorylation of STING serves as an upstream event, which facilitates the assembly of STING polymers upon DHN stimulation, thereby contributing to pyroptosis.

Although inhibition of cGAS did not affect DHN-induced PERK activation (Fig. S6D), it markedly impaired DHN-induced STING phosphorylation (Fig. S6O). Considering the essential role of cGAMP in STING function(47), we postulated that the interaction between cGAMP and STING may contribute to PERK-mediated phosphorylation of STING. Addition of cGAMP dramatically enhanced the phosphorylation of STING by PERK in an *in vitro* kinase assay (Fig. S6P). STING$^{R238A/Y240A}$, which lacks binding affinity for cGAMP(47), failed to undergo the DHN-induced phosphorylation (Fig. S6Q). Consequently, cells expressing STING$^{R238A/Y240A}$ were resistant to DHN-induced pyroptosis (Fig. S6R). Therefore, it appears that the interaction between STING and cGAMP functions as a structural priming event for subsequent PERK-mediated STING phosphorylation. In this context, both DHN-induced release of mtDNA (which activates cGAS to generate cGAMP) and intracellular acidity (required for PERK activation) are indispensable for the formation of ER-STING aggregates and induction of pyroptosis.

Pathological inhibitory effects of DHN on tumor growth in mice

To evaluate the *in vivo* antitumor efficacy of DHN, nude mice with A375 cell-derived xenografts were utilized. Intraperitoneal administration of DHN significantly suppressed the

growth of xenograft tumors, as evidenced by reduced tumor weight and size compared to the control group (Fig. 9A). It was also observed that DHN treatment significantly decreased the expression of Ki67, a marker of cell proliferation in tumors (Fig. 9B). The inhibitory effect of DHN was closely associated with GSDME cleavage (Fig. 9C) and the formation of punctate structures of STING (Fig. 9D) in tumor tissues. Furthermore, knockdown of CypD, the target protein of DHN, greatly impaired the suppressive effect of DHN on tumor growth as well as STING polymerization and GSDME cleavage (Fig. 9E-F), emphasizing the requirement of CypD for DHN effect. To further elucidate the involvement of STING and GSDME, nude mice bearing xenografts derived from A375 cells with knocked down STING or GSDME were also administered with DHN. As expected, knockdown of either STING or GSDME almost abolished the inhibitory effect exerted by DNH (Fig. 9G-H). Moreover, expression of $STING^{C206S}$ (abolishing STING polymerization) or $STING^{S345A/358A}$ (abolishing PERK-mediated STING phosphorylation) significantly attenuated the effect of DHN on tumor growth (Fig. 10A), accompanied with the decrease in STING polymerization and phosphorylation detected in the same tumor samples (Fig. 10B-C). Collectively, these results demonstrate that the inhibitory effect of DHN *in vivo* is indeed a result of pyroptosis induction and is closely associated with the CypD-STING-GSDME axis.

To further evaluate the anti-tumoral efficacy of DHN in immunocompetent mice models, we assessed its ability to induce pyroptosis in B16 (mouse melanoma cells) and Hepa1-6 (mouse hepatocellular carcinoma cells). Our findings demonstrated that DHN effectively induced STING oligomerization, GSDME cleavage, and pyroptosis in both cell lines (Fig. S7A). Subsequently, we employed B16 and Hepa1-6 cells to establish orthotopic xenografts in C57BL/6 immunocompetent mice. Our findings revealed that the administration of DHN markedly inhibited tumor growth derived from both B16 and Hepa1-6 cells (Fig. 10D). Notably, while DHN treatment had minimal impact on the proportions of CD4 T cells, CD8 T cells, or

natural killer (NK) cells within the tumor microenvironment, it markedly enhanced the activation status of these cells, as evidenced by increased proportions of interferon γ (IFNγ)$^+$, TNFα$^+$, perforin (PFN)$^+$, granzyme B (GZMB)$^+$/CD8 T cells, and IFNγ$^+$, PFN$^+$, GZMB$^+$/NK cells (Fig. 10E). Therefore, it could be concluded that this non-canonical cGAS-STING pathway-associated pyroptosis exhibits immunogenic properties and holds potential for inducing antitumor immune responses.

We finally assessed the PK/PD properties of DHN. To this end, we conducted a dosing study in the B16-derived xenograft model in C57BL/6 mice. The results demonstrated that a concentration of 20 mg/kg exhibited significant effect in suppressing xenograft growth. However, a concentration of 40 mg/kg did not yield more pronounced effects (Fig. S7B). Dose-related blood exposure of DHN in these mice was also observed, with a time at maximal concentration (T_{max}) of approximately 2 hours, correlating with dose-dependent exposure in tumor tissues. The half-life of DHN ($T_{1/2}$) was approximately 4.5 hours. Furthermore, DHN-induced GSDME cleavage in tumor tissues peaked at 24 hours post-injection (Fig. S7C), which aligns with the observation that DHN induces pyroptosis after 24 hours in melanoma cells, indicating its prolonged therapeutic effect. Notably, DHN administration at doses up to 40 mg/kg had a negligible effect on body weight. The weights and histological structures of the heart, liver, spleen, and kidney remained unchanged following DHN treatment. Plasma levels of CKMB (Creatine Kinase Myocardial Band, an indicator of cardiac injury), ALT and AST (Aspartate Aminotransferase and Alanine Aminotransferase, indicators of hepatic damage), and BUN (Blood Urea Nitrogen, an indicator of renal injury) showed minimal evidence of organ damage. Additionally, DHN did not affect colon length (Fig. S7D). Therefore, it can be concluded that DHN exhibits minimal toxicity in mice.

Discussion

The cGAS-STING signaling pathway has emerged as a pivotal mediator of innate immunity and is closely associated with anti-tumoral immune responses. STING agonists, either alone or in combination with immune checkpoint blockade therapy, are currently being clinically investigated for their potential efficacy in anticancer treatment. However, the direct induction of tumor cell death through manipulation of this pathway remains unknown. In this study, we identified a compound DHN that specifically induces pyroptosis in tumor cells through the non-canonical cGAS-STING pathway. On one hand, DHN targets CypD in the mitochondria to induce the opening of mPTP complex, resulting in the release of mtDNA into the cytoplasm where it activates cGAS to produce cGAMP. On the other hand, DHN causes intracellular acidification to activate PERK. The association of cGAMP with STING serves as a priming step for subsequent PERK-induced STING phosphorylation. This phosphorylation of STING not only retains it in the ER, but also facilitates its polymerization to form aggregates, thereby establishing a platform (i.e. ER-STING aggregates) to recruit caspase-8 and GSDME for further cleavage, ultimately triggering pyroptosis. Overall, our findings not only identify DHN as a pyroptosis inducer with promising implications for anti-tumor therapy, but also elucidate an alternative signaling pathway that connects non-canonical cGAS-STING pathway and acid environment to pyroptotic induction.

CypD, a well-established sensitizer of the mPTP, is a key component targeted by many pharmacological inhibitors including CsA, the gold-standard inhibitor of the mPTP(24). However, to the best of our knowledge, the existence of an activator specifically targeting CypD for mPTP opening remains unknown. In this study, we demonstrate DHN as an activator of mPTP through direct binding to CypD. Structurally, CsA specifically binds to the active site of CypD without interacting with the residues located in the S2 pocket, a substrate-binding groove adjacent to the active site(48, 49). In contrast, molecular modeling and point mutation

analysis suggest that the naphthalene ring of DHN interacts with residues near the active site, while its long hydrophobic carbon chain of DHN lies flat in the S2 pocket, exhibiting a distinct binding mode compared to CsA's interaction with CypD. This distinctive binding mode might generate an altered protein surface capable of modulating CypD's associations with binding partners. Considering the interaction between CypD and components of the mPTP complex, such as ATP synthase or ANT, regulates mPTP opening(24), it is plausible that DHN regulates the association between CypD and the mPTP complex to facilitate its opening, which warrants further investigation in the future. However, neither CsA treatment nor the knockdown of CypD or ANT1 completely abolishes mtDNA release upon DHN stimulation. This suggests that other factors may also partially participate in regulating DHN-induced mtDNA release.

The opening of mPTP is closely associated with the release of mtDNA into the cytosol, subsequently triggering innate immune responses by activating the cGAS-STING pathway(25, 50). While DHN-induced mPTP opening indeed stimulates mtDNA release and activates cGAS, it fails to activate the innate immune response, as evidenced by the absence of TBK1 and IRF3 phosphorylation, as well as transcriptional induction of type I interferons and interferon-stimulated genes, suggesting a non-canonical activation of the cGAS-STING pathway upon DHN stimulation. This may be attributed to PERK-mediated STING phosphorylation, which hinders STING translocation from ER to Golgi apparatus - a prerequisite for TBK1 and IRF3 activation(51). Previous studies have reported that transforming growth factor beta-activated kinase 1 (TAK1)-mediated phosphorylation at Ser355 is crucial for STING ER exit(52). Considering that in the current case, PERK phosphorylates STING at residues Ser345 and Ser358 in close proximity to TAK1 phosphorylation sites, it is not surprising that PERK-mediated phosphorylation could suppress STING ER exit. In this context, PERK-mediated phosphorylation may act as a functional switch determining whether STING remains in or exits from the ER.

The PERK-mediated retention of STING in the ER leads to non-canonical activation of STING, characterized by the formation of condensed membranous structures within the ER containing multi-protein complexes. This unique subcellular architecture recruits and processes GSDME cleavage by caspase-8 to induce pyroptosis, demonstrating a distinct compartmental regulation for pyroptosis induction. The formation of disulfide bonds at Cys206 is crucial for STING polymerization and subsequent assembly of ER-STING aggregates. In contrast, in the canonical cGAS-STING pathway, STING oligomerization is facilitated by disulfide bonds formed between Cys148 residues on each STING molecule(36). This discrepancy suggests that upon phosphorylation by PERK and retention in the ER, different residues are utilized by STING for polymerization, resulting in a distinct surface geometry necessary for recruiting specific binding partners such as caspase 8 and GSDME instead of TBK1 or IRF3. Consequently, this leads to the formation of ER-STING aggregates and induction of pyroptosis rather than activation of innate immunity. In this regards, Cys206 dependent STING polymerization favors non-canonical STING activation, which may partially explain the close association between individuals with mutations at Cys206 of STING and SAVI (STING-associated vasculopathy with onset in infancy), a disease characterized by systemic inflammation resulting from constitutive activation of the canonical STING pathway (53, 54).

DHN-induced PERK activation is not associated with mtDNA release and cGAS activation, but rather linked to the DHN-mediated intracellular acidification. Although the exact mechanism underlying this acidification is still not well understood, it is plausible that the weak acidic nature of DHN may at least partially contribute to it. Maintaining a constant intracellular pH is crucial for normal cellular functions since almost all cellular processes rely on a stable pH level(55, 56). Therefore, fluctuations in intracellular pH can modulate intracellular signaling transduction, and protons are considered second messengers in this context(57). In addition to DHN stimulation, we also found that a decrease in intracellular pH

was sufficient to activate PERK, suggesting that PERK could response to the decline of intracellular pH and connects the fluctuation of pH to the cGAS-STING pathway. However, considering that changes in intracellular acidity also impact protein folding(56), it is also plausible that PERK, being a key component of the unfolded protein response, gets activated indirectly under conditions of decreased pH.

DHN-induced acidification of the ER also plays a crucial role in the cleavage of GSDME by caspase-8 in the ER-STING aggregates. It has been suggested that caspase-8 promotes GSDME processing through activating caspase-3(5), however, our findings demonstrate that caspase-8 can directly cleave GSDME at Asp270 under acidic conditions, consistent with the optimal pH requirement for caspase-8 being less than 7(58). In this regard, the compartmental pH fluctuations within cells may serve as an overlooked regulatory pathway for caspase activation and cell death induction, warranting further investigation in future studies.

In summary, we found that DHN induces GSDME cleavage by caspase-8 and subsequent pyroptosis through activating a non-canonical cGAS-STING pathway, which relies on both cGAS activation and STING phosphorylation by PERK. Importantly, this non-canonical cGAS-STING pathway-associated pyroptosis is not limited to DHN stimulation; simultaneous activation of cGAS and reduction in intracellular acidity are sufficient for pyroptosis induction. Pathologically, given that glycolysis-generated lactic acid is one of the major contributors to intracellular acidity in tumors(59), the induction of cytoplasmic DNA in glycolysis-dependent tumor cells under conditions such as defects in the DNA damage response (DDR), chromosomal instability, replicative stress, reactivation of endogenous retroelements, or the release of mitochondrial DNA (60) may lead to atypical STING activation to some extent. This phenomenon warrants further investigation.

Methods

Additional details on methods can be found in the Supplemental Materials.

Sex as a biological variable

In this study, sex was not considered as a biological variable. All mice used in our study were male for easier handling and management purposes. It is unknown whether the findings are relevant for female mice.

Cell culture and transfection

The human melanoma cell line A375, murine melanoma cell line B16 and human hepatoma cell line Huh7 were obtained from Cell Bank in the Chinese Academy of Sciences. The human embryonic kidney cell line HEK293T, melanoma cell lines IgR3, M14, MEL-RM, human monocyte-like cell line THP-1, cervical cancer cell line HeLa, mouse hepatoma cell line Hepa1-6, human hepatoma cell line Plc, human kidney proximal tubule epithelial cell HK-2, human cardiomyocyte AC16, mouse cardiomyocyte HL-1, mouse myoblast cell line C2C12 and mouse fibroblast L929 were obtained from The American Type Culture Collection. The human melanoma cell line MV3 was obtained from Xiamen Immocell Biotechnology Co. The human ccRCC cell line 786-O was obtained from Procell Life Science&Technology. The primary mouse bone marrow-derived macrophages (BMDM) and bone marrow-derived dendritic cells (BMDC) were isolated from C57BL/6 mice. These cell lines were cultured in medium supplemented with 10% fetal bovine serum (FBS). During the drug treatment period, the FBS concentration was reduced from 10% to 2%. Cell transfection was performed using TurboFect transfection reagent (Thermo Fisher Scientific, Bremen Germany), except for HEK293T cells that were transfected using the calcium phosphate method.

Microscopy

Cells were seeded in 6-well plate at a confluency of 40%-60% and treated with various pharmacological agents to evaluate morphological alterations associated with pyroptosis. Subsequently, phase-contrast images were captured using a Nikon TE2000 microscope. For confocal microscopy, cells were rinsed with DMEM, fixed in 4% paraformaldehyde, blocked with blocking buffer (3% BSA and 0.2% Triton X-100) and subsequently incubated overnight at 4 °C with the appropriate primary antibody. Following cells were washed with washing buffer (0.2% BSA and 0.05% Triton X-100) and incubated with FITC or Texas Red-conjugated secondary antibodies (Life Technologies) for one hour at 37 °C. Nuclei were visualized by staining with 4′,6-diamidino-2-phenylindole (DAPI) at a concentration of 50 μg/mL for five minutes. Confocal images were acquired using a Zeiss LSM 980 confocal microscope. For phase separation of depolymerization assay, cells were treated with 5% 1,6-hexanediol for 10 minutes to induce phase separation, followed by processing as described for confocal microscopy.

LDH release assay

The activity of lactate dehydrogenase (LDH) released into the cell culture supernatants was measured using the CytoTox 96 Non-Radioactive Cytotoxicity Assay Kit (Promega) to assess pyroptosis, according to the manufacturer's instructions.

Immunoblotting

Cells were lysed using ELB lysis buffer (containing 150 mM NaCl, 100 mM NaF, 50 mM Tris-HCl at pH 7.6, and 0.5% Nonidet P-40 (NP-40)), supplemented with a cocktail of protease inhibitor and phosphatase inhibitor. After centrifugation of the cell lysates at 14,000× g at 4 °C for 15 minutes, the supernatants were combined with an equal volume of 2× SDS loading buffer

and boiled for 15 minutes. Subsequently, the samples underwent SDS-PAGE followed by transfer onto a PVDF membrane for immunoblotting analysis using specific antibodies. For STING polymer analysis, samples were prepared with or without β-mercaptoethanol in both reduced and non-reduced forms. Cell lysates were collected in 2× SDS loading buffer excluding β-mercaptoethanol. Subsequently, the samples were separated using either SDS-PAGE or 4%–12% gradient gel electrophoresis.

Mouse models

Male BALB/c nude mice (7-8 weeks old, weighing 18-22 g) and C57BL/6J (7–8 weeks old) mice were procured from the SLAC Laboratory Animal Center in China and housed at the Laboratory Animal Center of Xiamen University (China). They were housed in a controlled environment with a 12-hour light-dark cycle and provided ad libitum access to food and water.

The A375 cell xenograft tumor model was established by subcutaneously injecting 1×10^6 A375 cells in 100 μL DMEM into the anterior flanks of BALB/c nude mice. After 4 days, the mice were divided into different groups: treatment with vehicle (10% DMSO in saline, 100 μL per mouse) or DHN (20 mg/kg; DHN dissolved in 10% DMSO and further diluted with saline) via intraperitoneal injections every other day for 2 weeks. Subsequently, the mice were euthanized, and their body weights as well as tumor weights were recorded.

The B16 cell xenograft tumor model was established by subcutaneously injecting 1×10^5 B16 cells in 100 μL DMEM into the anterior flanks of C57BL/6J mice. After 4 days, the mice were divided into different groups: treatment with vehicle (10% DMSO in saline, 100 μL per mouse) or DHN (20 mg/kg; DHN dissolved in 10% DMSO and further diluted with saline) via intraperitoneal injections once daily for 1 week. Subsequently, the mice were euthanized, and their body weights as well as tumor weights were recorded.

The Hepa1-6 cell orthotopic xenograft tumor model was established by subcutaneously injecting 2×10^6 Hepa1-6 cells into the subcapsular region of the left liver lobe of C57BL/6J mice. After 4 days, the mice were divided into different groups: treatment with vehicle (10% DMSO in saline, 100 μL per mouse) or DHN (20 mg/kg; DHN dissolved in 10% DMSO and further diluted with saline) via intraperitoneal injections once daily for 2 weeks. Subsequently, the mice were euthanized, and their body weights as well as tumor weights were recorded.

Statistical analysis

The statistical analyses were conducted using GraphPad Prism 9 software. The data are presented as means ± SEM. For the comparison between two groups, a two-tailed Student's t-test was employed. To assess differences among multiple groups, one-way analysis of variance (ANOVA) with Tukey's multiple comparisons test and two-way ANOVA with Tukey's multiple comparisons test was performed.

Study approval

The experimental protocols involving animals were approved by the Xiamen University Animal Ethics Committee (Approval No: XMULAC20220044).

Data availability

All data generated or analyzed in this study are included in this manuscript and its supplementary information files. Numerical values underlying graphical representations are provided in the Supplemental Supporting Data Values file.

Author Contributions

L.X., Y.L.A. and X.Y.M. performed experiments and analyzed data; H.L. and F.N.L. were responsible for the design of the compound DHN; T.G. completed synthesis of the compound DHN. X.Z. and X.M.D. helped design and synthesize the probe DHN-P; L.Z.W., Q.T.C. and B.Z. provided technical advice about experimental design and joined the discussion; W.B.H. carried out the molecular docking analysis; L.M.Y. provided transmission electron microscope technical support and data analysis; J.J.C. provided technical support and data analysis for SPR and FL-DSF; L.X., Y.L.A., Q.W. and H.Z.C. designed experiments, wrote the manuscript, and prepared the final scheme presentation. Q.W. and H.Z.C. jointly supervised this work. All authors have read and approved the article.

Acknowledgements

We are grateful to Prof. Jiahuai Han from School of Life Sciences, Xiamen University, Fujian, China, for providing HSV-1, and to Prof. Pinglong Xu from Life Sciences Institute, Zhejiang University, Zhejiang, China, for providing the plasmids of cGAS and STING. This work was supported by grants from the National Natural Science Foundation of China (9225330012, U23A20450, 32170777, 22025702, 22494692 and 82021003) and the Natural Science Foundation of Fujian Province, China (2024J01021).

References

1. Shi J, Gao W, and Shao F. Pyroptosis: Gasdermin-Mediated Programmed Necrotic Cell Death. *Trends Biochem Sci.* 2017;42(4):245-54.
2. Zhang JY, Zhou B, Sun RY, Ai YL, Cheng K, Li FN, et al. The metabolite α-KG induces GSDMC-dependent pyroptosis through death receptor 6-activated caspase-8. *Cell Res.* 2021;31(9):980-97.
3. Hou J, Zhao R, Xia W, Chang CW, You Y, Hsu JM, et al. PD-L1-mediated gasdermin C expression switches apoptosis to pyroptosis in cancer cells and facilitates tumour necrosis. *Nat Cell Biol.* 2020;22(10):1264-75.
4. Shi J, Zhao Y, Wang K, Shi X, Wang Y, Huang H, et al. Cleavage of GSDMD by inflammatory caspases determines pyroptotic cell death. *Nature.* 2015;526(7575):660-5.

5. Sarhan J, Liu BC, Muendlein HI, Li P, Nilson R, Tang AY, et al. Caspase-8 induces cleavage of gasdermin D to elicit pyroptosis during Yersinia infection. *Proceedings of the National Academy of Sciences of the United States of America.* 2018;115(46):E10888-e97.
6. Wang Y, Gao W, Shi X, Ding J, Liu W, He H, et al. Chemotherapy drugs induce pyroptosis through caspase-3 cleavage of a gasdermin. *Nature.* 2017;547(7661):99-103.
7. Zhou B, Zhang JY, Liu XS, Chen HZ, Ai YL, Cheng K, et al. Tom20 senses iron-activated ROS signaling to promote melanoma cell pyroptosis. *Cell Res.* 2018;28(12):1171-85.
8. Ai YL, Wang WJ, Liu FJ, Fang W, Chen HZ, Wu LZ, et al. Mannose antagonizes GSDME-mediated pyroptosis through AMPK activated by metabolite GlcNAc-6P. *Cell Res.* 2023;33(12):904-22.
9. Zhang Z, Zhang Y, Xia S, Kong Q, Li S, Liu X, et al. Gasdermin E suppresses tumour growth by activating anti-tumour immunity. *Nature.* 2020;579(7799):415-20.
10. Hopfner KP, and Hornung V. Molecular mechanisms and cellular functions of cGAS-STING signalling. *Nature reviews Molecular cell biology.* 2020;21(9):501-21.
11. Woo SR, Fuertes MB, Corrales L, Spranger S, Furdyna MJ, Leung MY, et al. STING-dependent cytosolic DNA sensing mediates innate immune recognition of immunogenic tumors. *Immunity.* 2014;41(5):830-42.
12. Gaidt MM, Ebert TS, Chauhan D, Ramshorn K, Pinci F, Zuber S, et al. The DNA Inflammasome in Human Myeloid Cells Is Initiated by a STING-Cell Death Program Upstream of NLRP3. *Cell.* 2017;171(5):1110-24.e18.
13. Woo MS, Mayer C, Binkle-Ladisch L, Sonner JK, Rosenkranz SC, Shaposhnykov A, et al. STING orchestrates the neuronal inflammatory stress response in multiple sclerosis. *Cell.* 2024.
14. Cai Y, Chen X, Lu T, Fang X, Ding M, Yu Z, et al. Activation of STING by SAMHD1 Deficiency Promotes PANoptosis and Enhances Efficacy of PD-L1 Blockade in Diffuse Large B-cell Lymphoma. *Int J Biol Sci.* 2023;19(14):4627-43.
15. Zhang W, Li G, Luo R, Lei J, Song Y, Wang B, et al. Cytosolic escape of mitochondrial DNA triggers cGAS-STING-NLRP3 axis-dependent nucleus pulposus cell pyroptosis. *Exp Mol Med.* 2022;54(2):129-42.
16. Wu S, Wang B, Li H, Wang H, Du S, Huang X, et al. Targeting STING elicits GSDMD-dependent pyroptosis and boosts anti-tumor immunity in renal cell carcinoma. *Oncogene.* 2024;43(20):1534-48.
17. Hetz C, Zhang K, and Kaufman RJ. Mechanisms, regulation and functions of the unfolded protein response. *Nature reviews Molecular cell biology.* 2020;21(8):421-38.
18. Zhang D, Liu Y, Zhu Y, Zhang Q, Guan H, Liu S, et al. A non-canonical cGAS-STING-PERK pathway facilitates the translational program critical for senescence and organ fibrosis. *Nat Cell Biol.* 2022;24(5):766-82.
19. Wang WJ, Wang Y, Chen HZ, Xing YZ, Li FW, Zhang Q, et al. Orphan nuclear receptor TR3 acts in autophagic cell death via mitochondrial signaling pathway. *Nat Chem Biol.* 2014;10(2):133-40.
20. Zhan Y, Du X, Chen H, Liu J, Zhao B, Huang D, et al. Cytosporone B is an agonist for nuclear orphan receptor Nur77. *Nat Chem Biol.* 2008;4(9):548-56.
21. Muzio M, Stockwell BR, Stennicke HR, Salvesen GS, and Dixit VM. An induced proximity model for caspase-8 activation. *J Biol Chem.* 1998;273(5):2926-30.
22. Zhou B, Jiang ZH, Dai MR, Ai YL, Xiao L, Zhong CQ, et al. Full-length GSDME mediates pyroptosis independent from cleavage. *Nat Cell Biol.* 2024.
23. Yang R, Zhang Y, Geng B, Tian Y, Tian W, Zou Y, et al. Fluorescence labeling-based differential scanning fluorimetry, an effective method for protein thermal stability and protein-compound binding analysis. *Int J Biol Macromol.* 2024;281(Pt 1):136043.
24. Izzo V, Bravo-San Pedro JM, Sica V, Kroemer G, and Galluzzi L. Mitochondrial Permeability Transition: New Findings and Persisting Uncertainties. *Trends Cell Biol.* 2016;26(9):655-67.
25. Xian H, Watari K, Sanchez-Lopez E, Offenberger J, Onyuru J, Sampath H, et al. Oxidized DNA fragments exit mitochondria via mPTP- and VDAC-dependent channels to activate NLRP3 inflammasome and interferon signaling. *Immunity.* 2022;55(8):1370-85.e8.
26. García N, and Chávez E. Mitochondrial DNA fragments released through the permeability transition pore correspond to specific gene size. *Life Sci.* 2007;81(14):1160-6.
27. Kwong JQ, and Molkentin JD. Physiological and pathological roles of the mitochondrial permeability transition pore in the heart. *Cell Metab.* 2015;21(2):206-14.
28. Bernardi P, Gerle C, Halestrap AP, Jonas EA, Karch J, Mnatsakanyan N, et al. Identity, structure, and function of the mitochondrial permeability transition pore: controversies, consensus, recent advances, and future directions. *Cell Death Differ.* 2023;30(8):1869-85.
29. Du M, and Chen ZJ. DNA-induced liquid phase condensation of cGAS activates innate immune signaling. *Science.* 2018;361(6403):704-9.

30. Lama L, Adura C, Xie W, Tomita D, Kamei T, Kuryavyi V, et al. Development of human cGAS-specific small-molecule inhibitors for repression of dsDNA-triggered interferon expression. *Nat Commun.* 2019;10(1):2261.
31. Thomson DW, Poeckel D, Zinn N, Rau C, Strohmer K, Wagner AJ, et al. Discovery of GSK8612, a Highly Selective and Potent TBK1 Inhibitor. *ACS medicinal chemistry letters.* 2019;10(5):780-5.
32. Yu X, Zhang L, Shen J, Zhai Y, Jiang Q, Yi M, et al. The STING phase-separator suppresses innate immune signalling. *Nat Cell Biol.* 2021;23(4):330-40.
33. Tanaka Y, and Chen ZJ. STING specifies IRF3 phosphorylation by TBK1 in the cytosolic DNA signaling pathway. *Sci Signal.* 2012;5(214):ra20.
34. Yuan J, and Ofengeim D. A guide to cell death pathways. *Nat Rev Mol Cell Biol.* 2024;25(5):379-95.
35. Wang W, and Roberts CJ. Protein aggregation - Mechanisms, detection, and control. *Int J Pharm.* 2018;550(1-2):251-68.
36. Ergun SL, Fernandez D, Weiss TM, and Li L. STING Polymer Structure Reveals Mechanisms for Activation, Hyperactivation, and Inhibition. *Cell.* 2019;178(2):290-301.e10.
37. Zamorano Cuervo N, Fortin A, Caron E, Chartier S, and Grandvaux N. Pinpointing cysteine oxidation sites by high-resolution proteomics reveals a mechanism of redox-dependent inhibition of human STING. *Sci Signal.* 2021;14(680).
38. Sun L, Wu J, Du F, Chen X, and Chen ZJ. Cyclic GMP-AMP synthase is a cytosolic DNA sensor that activates the type I interferon pathway. *Science (New York, NY).* 2013;339(6121):786-91.
39. Casey JR, Grinstein S, and Orlowski J. Sensors and regulators of intracellular pH. *Nat Rev Mol Cell Biol.* 2010;11(1):50-61.
40. Chiche J, Brahimi-Horn MC, and Pouysségur J. Tumour hypoxia induces a metabolic shift causing acidosis: a common feature in cancer. *J Cell Mol Med.* 2010;14(4):771-94.
41. Estrella V, Chen T, Lloyd M, Wojtkowiak J, Cornnell HH, Ibrahim-Hashim A, et al. Acidity generated by the tumor microenvironment drives local invasion. *Cancer Res.* 2013;73(5):1524-35.
42. Li X, Yang Y, Zhang B, Lin X, Fu X, An Y, et al. Lactate metabolism in human health and disease. *Signal Transduct Target Ther.* 2022;7(1):305.
43. Bridgeman A, Maelfait J, Davenne T, Partridge T, Peng Y, Mayer A, et al. Viruses transfer the antiviral second messenger cGAMP between cells. *Science.* 2015;349(6253):1228-32.
44. Ma K, Vattem KM, and Wek RC. Dimerization and release of molecular chaperone inhibition facilitate activation of eukaryotic initiation factor-2 kinase in response to endoplasmic reticulum stress. *The Journal of biological chemistry.* 2002;277(21):18728-35.
45. PhosphoSitePlus. [Database]. https://www.phosphosite.org. Accessed July 30, 2023.
46. Hornbeck PV, Zhang B, Murray B, Kornhauser JM, Latham V, and Skrzypek E. PhosphoSitePlus, 2014: mutations, PTMs and recalibrations. *Nucleic Acids Res.* 2015;43(Database issue):D512-20.
47. Shang G, Zhang C, Chen ZJ, Bai XC, and Zhang X. Cryo-EM structures of STING reveal its mechanism of activation by cyclic GMP-AMP. *Nature.* 2019;567(7748):389-93.
48. Kajitani K, Fujihashi M, Kobayashi Y, Shimizu S, Tsujimoto Y, and Miki K. Crystal structure of human cyclophilin D in complex with its inhibitor, cyclosporin A at 0.96-A resolution. *Proteins.* 2008;70(4):1635-9.
49. Peterson AA, Rangwala AM, Thakur MK, Ward PS, Hung C, Outhwaite IR, et al. Discovery and molecular basis of subtype-selective cyclophilin inhibitors. *Nat Chem Biol.* 2022;18(11):1184-95.
50. Yu CH, Davidson S, Harapas CR, Hilton JB, Mlodzianoski MJ, Laohamonthonkul P, et al. TDP-43 Triggers Mitochondrial DNA Release via mPTP to Activate cGAS/STING in ALS. *Cell.* 2020;183(3):636-49.e18.
51. Fang R, Jiang Q, Guan Y, Gao P, Zhang R, Zhao Z, et al. Golgi apparatus-synthesized sulfated glycosaminoglycans mediate polymerization and activation of the cGAMP sensor STING. *Immunity.* 2021;54(5):962-75.e8.
52. Ma M, Dang Y, Chang B, Wang F, Xu J, Chen L, et al. TAK1 is an essential kinase for STING trafficking. *Mol Cell.* 2023;83(21):3885-903.e5.
53. Zhang X, Bai XC, and Chen ZJ. Structures and Mechanisms in the cGAS-STING Innate Immunity Pathway. *Immunity.* 2020;53(1):43-53.
54. Seo J, Kang JA, Suh DI, Park EB, Lee CR, Choi SA, et al. Tofacitinib relieves symptoms of stimulator of interferon genes (STING)-associated vasculopathy with onset in infancy caused by 2 de novo variants in TMEM173. *J Allergy Clin Immunol.* 2017;139(4):1396-9.e12.
55. Jin X, Zhou M, Chen S, Li D, Cao X, and Liu B. Effects of pH alterations on stress- and aging-induced protein phase separation. *Cellular and molecular life sciences : CMLS.* 2022;79(7):380.
56. Orij R, Brul S, and Smits GJ. Intracellular pH is a tightly controlled signal in yeast. *Biochimica et biophysica acta.* 2011;1810(10):933-44.

57. Isom DG, Sridharan V, Baker R, Clement ST, Smalley DM, and Dohlman HG. Protons as second messenger regulators of G protein signaling. *Molecular cell.* 2013;51(4):531-8.
58. Stennicke HR, and Salvesen GS. Biochemical characteristics of caspases-3, -6, -7, and -8. *J Biol Chem.* 1997;272(41):25719-23.
59. Yamagata M, Hasuda K, Stamato T, and Tannock IF. The contribution of lactic acid to acidification of tumours: studies of variant cells lacking lactate dehydrogenase. *Br J Cancer.* 1998;77(11):1726-31.
60. Samson N, and Ablasser A. The cGAS-STING pathway and cancer. *Nat Cancer.* 2022;3(12):1452-63.

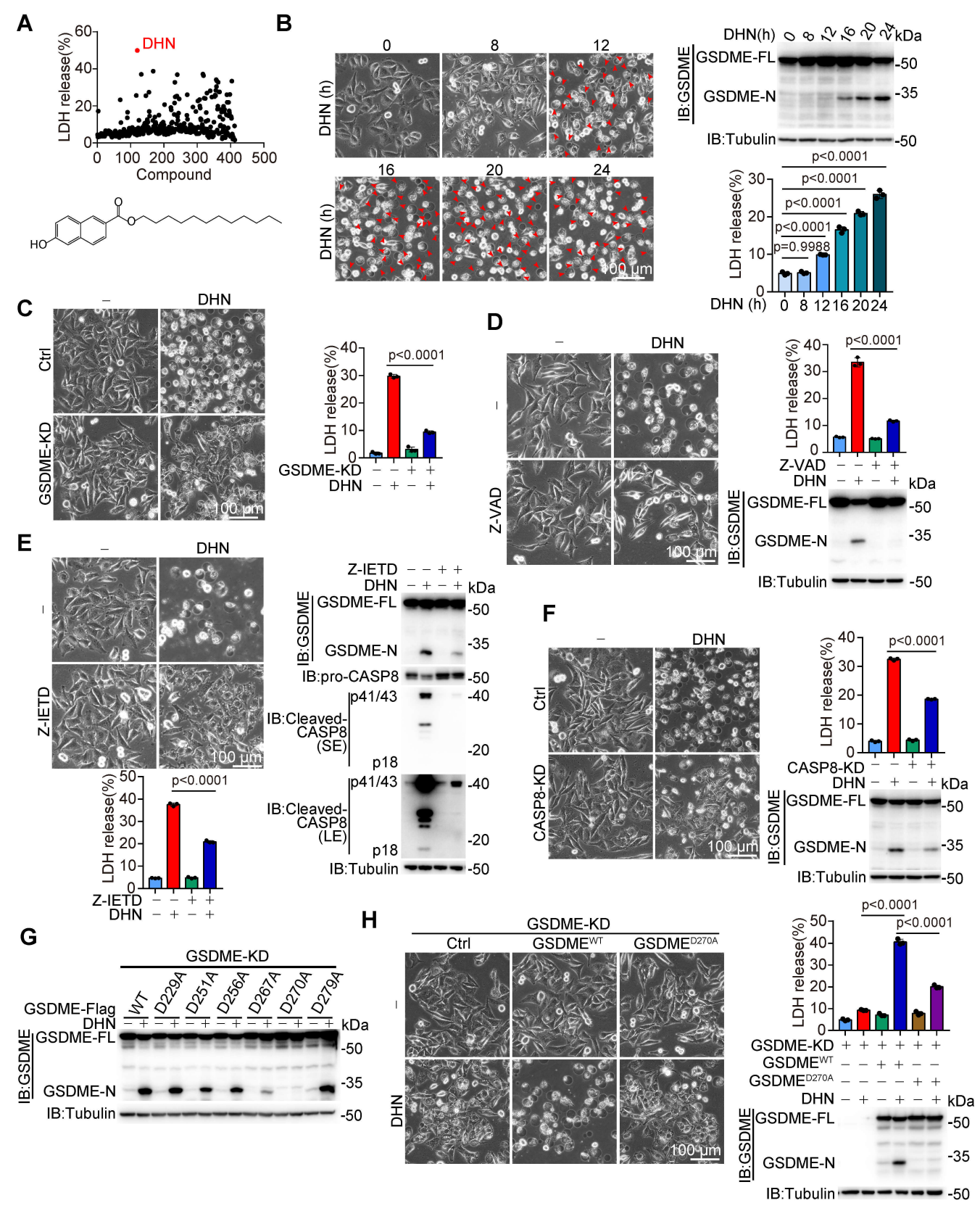
A
LDH release(%)
DHN
Compound
HO
B
DHN (h)
0
8
12
16
20
24
100 μm
IB:GSDME
GSDME-FL
GSDME-N
IB:Tubulin
kDa
-50
-35
p<0.0001
p=0.9988
LDH release(%)
C
Ctrl
GSDME-KD
DHN
D
Z-VAD
E
Z-IETD
IB:pro-CASP8
IB:Cleaved-CASP8 (SE)
IB:Cleaved-CASP8 (LE)
p41/43
p18
F
CASP8-KD
G
GSDME-KD
GSDME-Flag
WT
D229A
D251A
D256A
D267A
D270A
D279A
H
Ctrl
GSDME^WT
GSDME^D270A

Fig. 1 DHN induces pyroptosis by caspase-8-mediated cleavage of GSDME. Melanoma A375 cells were treated with DHN (15 μM) for 20 hours to assess pyroptotic features (including characteristic morphology, GSDME cleavage, and LDH release), unless specifically defined. **A** Compound library screening and chemical structure of DHN. **B** DHN induced pyroptosis at different time points and cells with characteristic pyroptotic morphology were indicated by red arrows. The cleavage of GSDME was detected by Western blot, and cell death was evaluated by accessing LDH release. **C-F** GSDME (**C**) or Caspase8 (**F**) was separately knocked down in cells or cells were co-treated with Z-VAD (**D**, 20 μM) or Z-IETD (**E**, 10 μM), followed by detection of pyroptosis. **G** $GSDME^{WT}$, $GSDME^{D229A}$, $GSDME^{D251A}$, $GSDME^{D256A}$, $GSDME^{D267A}$, $GSDME^{D270A}$ or $GSDME^{D279A}$ was separately transfected into GSDME-knockdown cells, then the cleavage level of GSDME was detected. **H** $GSDME^{WT}$ or $GSDME^{D270A}$ was separately transfected into GSDME-knockdown cells, then pyroptosis was detected. Tubulin was used to determine the amount of loading proteins. Statistical data are presented as mean ± s.e.m. of (n = 3) three independent experiments. Statistical analyses were determined by one-way analysis of variance (ANOVA) with Tukey's multiple comparisons test (**B**) and two-way ANOVA with Tukey's multiple comparisons test (**C-F**, **H**). P values are indicated. All western blots were repeated at least twice and one of them is shown. IB, immunoblot; KD, knockdown; WT, wild-type; SE, short exposure; LE, long exposure.

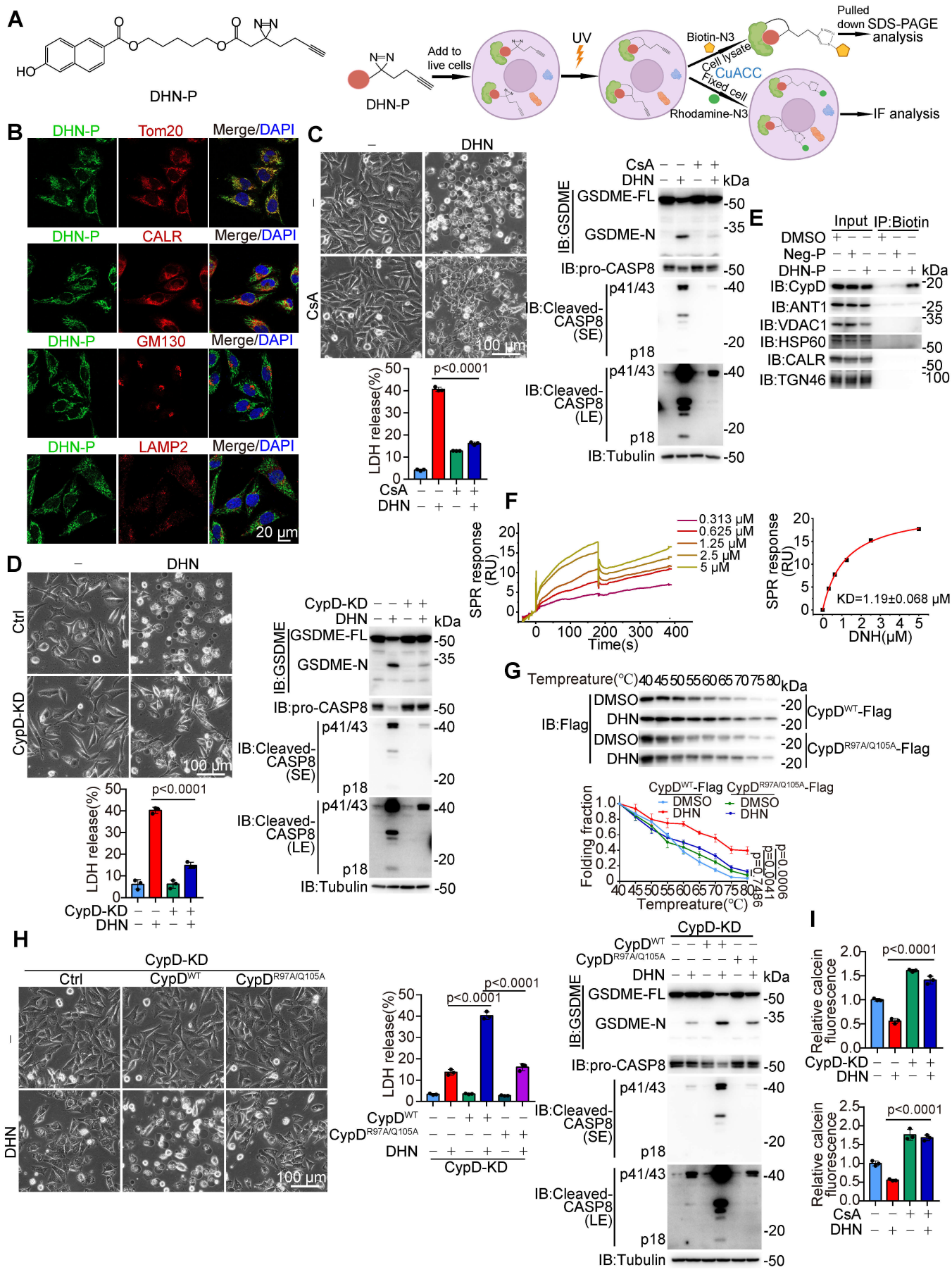
A
DHN-P
Add to live cells
UV
Biotin-N3
Cell lysate
CuACC
Fixed cell
Rhodamine-N3
Pulled down SDS-PAGE analysis
IF analysis
B
DHN-P
Tom20
CALR
GM130
LAMP2
Merge/DAPI
20 μm
C
DHN
CsA
100 μm
LDH release(%)
p<0.0001
IB:GSDME
GSDME-FL
GSDME-N
IB:pro-CASP8
IB:Cleaved-CASP8 (SE)
IB:Cleaved-CASP8 (LE)
p41/43
p18
IB:Tubulin
kDa
E
Input
IP:Biotin
DMSO
Neg-P
DHN-P
IB:CypD
IB:ANT1
IB:VDAC1
IB:HSP60
IB:CALR
IB:TGN46
F
SPR response (RU)
Time(s)
0.313 μM
0.625 μM
1.25 μM
2.5 μM
5 μM
KD=1.19±0.068 μM
DNH(μM)
D
Ctrl
CypD-KD
100 μm
G
Tempreature(℃)
IB:Flag
CypD^WT-Flag
CypD^R97A/Q105A-Flag
Folding fraction
p=0.0006
p=0.0041
p=0.0076
H
CypD-KD
Ctrl
CypD^WT
CypD^R97A/Q105A
I
Relative calcein fluorescence

Fig. 2 DHN promotes the opening of mPTP by targeting mitochondrial protein CypD. Melanoma A375 cells were treated with DHN (15 μM) for 20 hours to assess pyroptotic features (including characteristic morphology, caspase8/GSDME cleavage, and LDH release), unless specifically defined. **A** Chemical structure of DHN probe (DHN-P, left) and workflow of click chemistry for DHN-P (right). **B** Cells were treated with DHN-P (150 μM) for 2 hours. Azide-rhodamine was conjugated with DHN-P, and the localization of DHN-P was shown (Tom20: mitochondria marker; CALR: ER marker; GM130: Golgi marker; LAMP2: lysosomal marker). **C, D** Cells were treated with DHN in the presence of CsA (**C**, 5 μM) or in CypD knockdown cells (**D**), followed by the detection of pyroptosis. **E** Cells were treated with DHN-P (150 μM) for 2 hours, azide-biotin was added to conjugate with DHN-P. The DHN-P-targeted CypD was assayed by streptavidin beads. **F** The binding affinity between DHN and CypD was determined by SPR. **G** Cellular thermal shift assay (CETSA). The protein of $CypD^{WT}$ or $CypD^{R97A/Q105A}$ were immunoprecipitated from cells, followed by treatment with DHN and subsequent differential temperature incubation for 15 minutes. Resulting lysates were subjected to western blot analysis. **H** $CypD^{WT}$ or $CypD^{R97A/Q105A}$ was separately transfected into CypD-knockdown cells, followed by the detection of pyroptosis. **I** CypD was knocked down in cells or cells were co-treated with CsA (5 μM) for 12 hours, followed by the detection of the opening of mPTP. Tubulin was used to determine the amount of loading proteins. DAPI wasused to indicate nucleus in confocal microscopy. Statistical data are presented as mean ± s.e.m. of (n = 3) three independent experiments. Statistical analyses were determined by two-way ANOVA with Tukey's multiple comparisons test (**C**, **D, G, H, I**). P values are indicated. All western blots were repeated at least twice and one of them is shown.

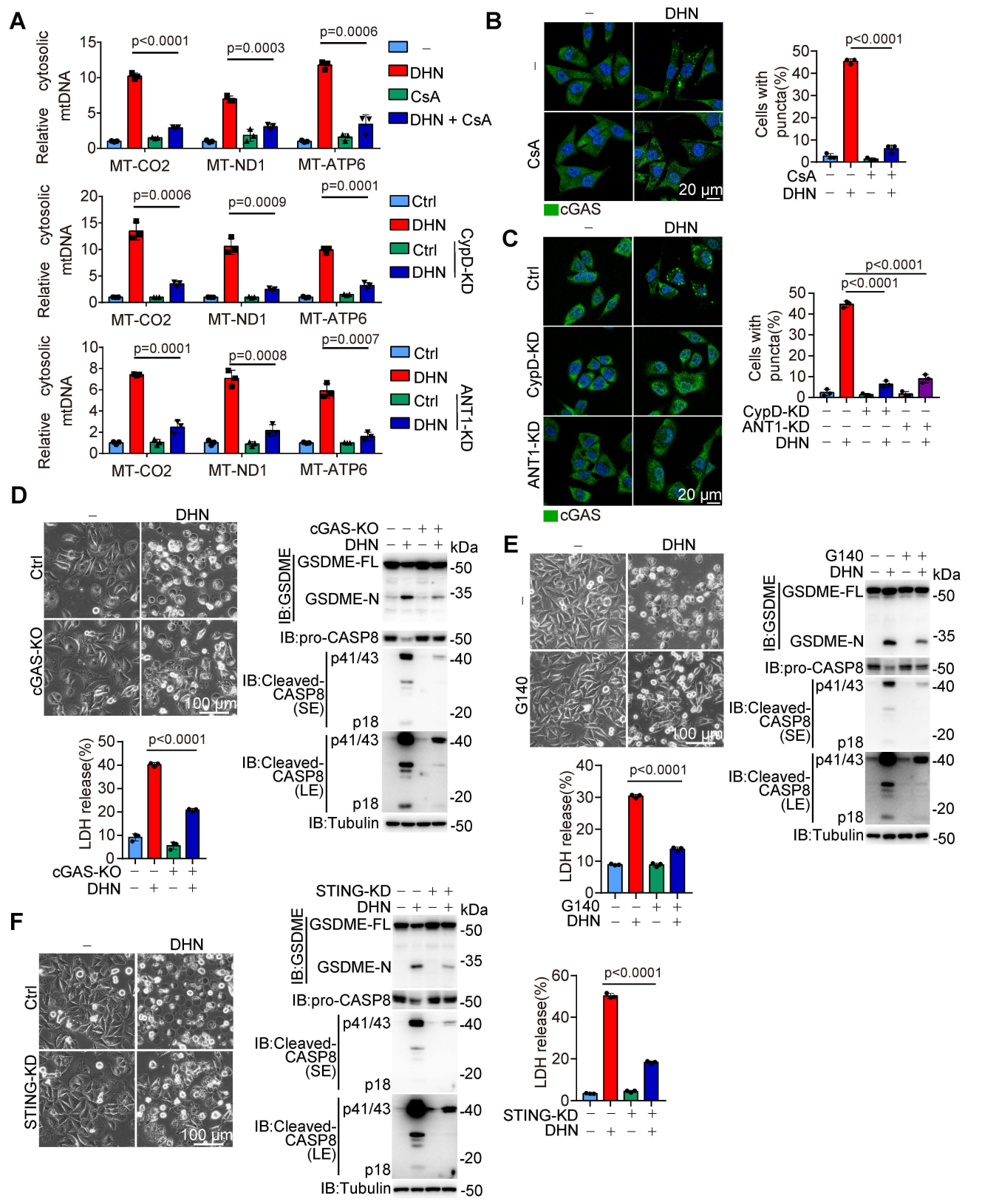
A
Relative cytosolic mtDNA
p<0.0001
p=0.0003
p=0.0006
–
DHN
CsA
DHN + CsA
MT-CO2
MT-ND1
MT-ATP6
p=0.0006
p=0.0009
p=0.0001
Ctrl
DHN
Ctrl
DHN
CypD-KD
p=0.0001
p=0.0008
p=0.0007
Ctrl
DHN
Ctrl
DHN
ANT1-KD
B
DHN
CsA
cGAS
20 μm
Cells with puncta(%)
p<0.0001
CsA
DHN
C
DHN
Ctrl
CypD-KD
ANT1-KD
cGAS
20 μm
p<0.0001
p<0.0001
Cells with puncta(%)
CypD-KD
ANT1-KD
DHN
D
DHN
Ctrl
cGAS-KO
100 μm
cGAS-KO
DHN
kDa
IB:GSDME
GSDME-FL
GSDME-N
IB:pro-CASP8
IB:Cleaved-CASP8 (SE)
IB:Cleaved-CASP8 (LE)
p41/43
p18
IB:Tubulin
-50
-35
-40
-20
LDH release(%)
p<0.0001
cGAS-KO
DHN
E
DHN
G140
100 μm
G140
DHN
kDa
IB:GSDME
GSDME-FL
GSDME-N
IB:pro-CASP8
IB:Cleaved-CASP8 (SE)
IB:Cleaved-CASP8 (LE)
p41/43
p18
IB:Tubulin
LDH release(%)
p<0.0001
G140
DHN
F
DHN
Ctrl
STING-KD
100 μm
STING-KD
DHN
kDa
IB:GSDME
GSDME-FL
GSDME-N
IB:pro-CASP8
IB:Cleaved-CASP8 (SE)
IB:Cleaved-CASP8 (LE)
p41/43
p18
IB:Tubulin
LDH release(%)
p<0.0001
STING-KD
DHN

Fig. 3 DHN-induced mtDNA release activates the cytosolic cGAS. Melanoma A375 cells were treated with DHN (15 μM) for 12 hours to show the puncta of cGAS and detect the release of mtDNA, for 20 h to assess pyroptotic features (including characteristic morphology, caspase8/GSDME cleavage, and LDH release), unless specifically defined. **A** Cells were co-treated with CsA (top, 5 μM), and CypD (middle) or ANT1 (bottom) was knocked down in cells, followed by detection of mtDNA release. **B-C** Cells were co-treated with CsA (**B**, 5 μM), and CypD or ANT1 (**C**) was knocked down in cells, then stained with anti-cGAS antibody. cGAS puncta were observed under confocal microscope. The percentage of cells with cGAS puncta was quantified (right, mean ± s.e.m., n = 3 repeats). The quantification and counting of 100 cells were performed three times in a single experiment, and the average value obtained from the three statistical measurements was recorded as one repetition. **D-F** Cells were co-treated with G140 (**E**, 30 μM), cGAS was knocked out (**D**) or STING was knocked down (**F**) in cells, followed by the detection of pyroptosis. Tubulin was used to determine the amount of loading proteins. Statistical data are presented as mean ± s.e.m. of (n = 3) three independent experiments. Statistical analyses were determined by two-way ANOVA with Tukey's multiple comparisons test (**A-F**). P values are indicated. All western blots were repeated at least twice and one of them is shown.

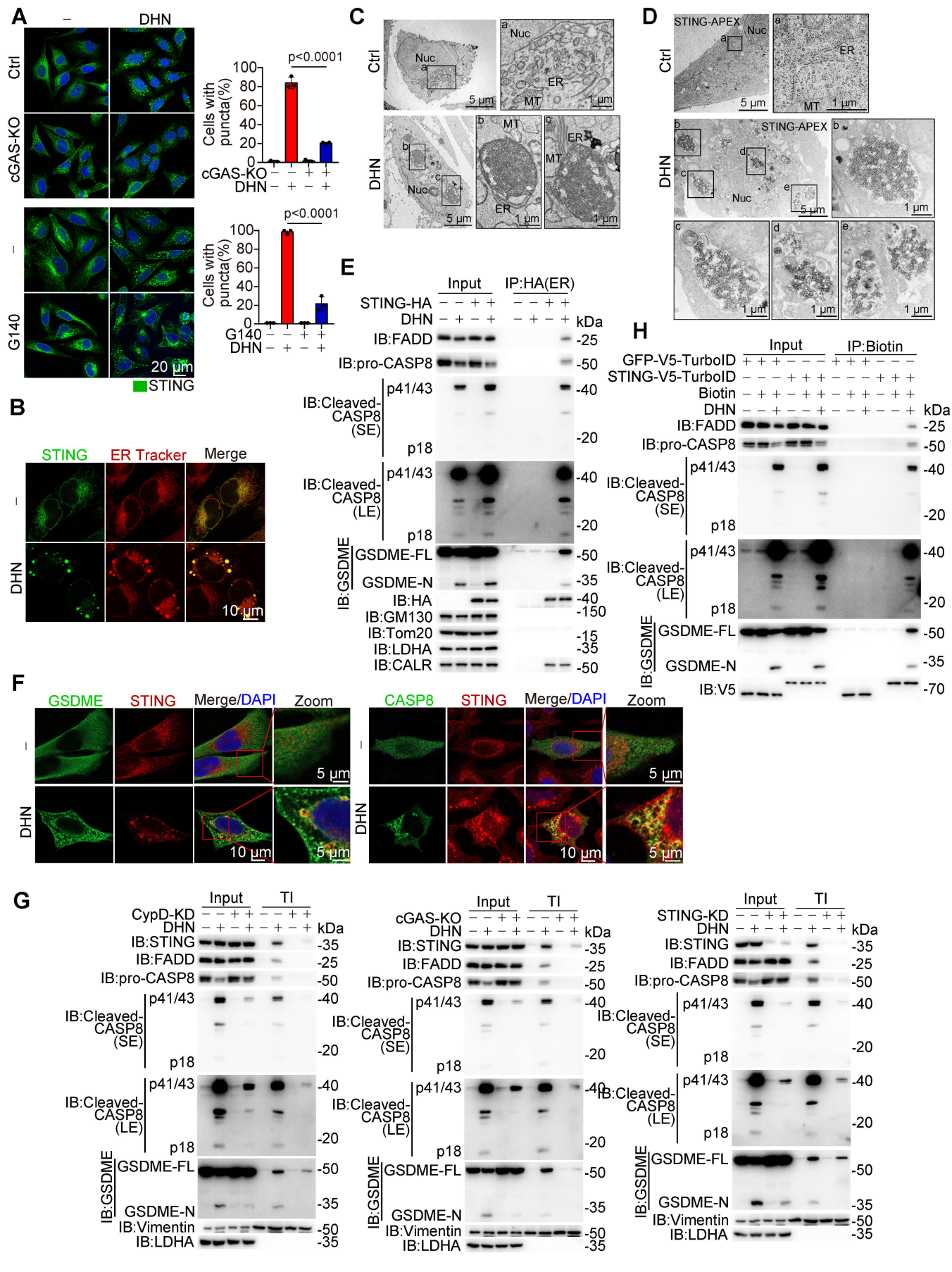
A
–
DHN
Ctrl
cGAS-KO
–
G140
20 μm
STING
p<0.0001
Cells with puncta(%)
cGAS-KO
DHN
p<0.0001
Cells with puncta(%)
G140
DHN
B
STING
ER Tracker
Merge
–
DHN
10 μm
C
Ctrl
DHN
Nuc
ER
MT
5 μm
1 μm
D
STING-APEX
Ctrl
DHN
Nuc
ER
MT
5 μm
1 μm
E
Input
IP:HA(ER)
STING-HA
DHN
kDa
IB:FADD
IB:pro-CASP8
IB:Cleaved-CASP8 (SE)
IB:Cleaved-CASP8 (LE)
p41/43
p18
IB:GSDME
GSDME-FL
GSDME-N
IB:HA
IB:GM130
IB:Tom20
IB:LDHA
IB:CALR
H
Input
IP:Biotin
GFP-V5-TurboID
STING-V5-TurboID
Biotin
DHN
kDa
IB:FADD
IB:pro-CASP8
IB:Cleaved-CASP8 (SE)
IB:Cleaved-CASP8 (LE)
p41/43
p18
IB:GSDME
GSDME-FL
GSDME-N
IB:V5
F
GSDME
STING
Merge/DAPI
Zoom
CASP8
STING
Merge/DAPI
Zoom
–
DHN
5 μm
10 μm
G
Input
TI
CypD-KD
cGAS-KO
STING-KD
DHN
kDa
IB:STING
IB:FADD
IB:pro-CASP8
IB:Cleaved-CASP8 (SE)
IB:Cleaved-CASP8 (LE)
p41/43
p18
IB:GSDME
GSDME-FL
GSDME-N
IB:Vimentin
IB:LDHA

Fig.4 DHN induces the formation of STING aggregates to recruit caspase-8 and GSDME. Melanoma A375 cells were treated with DHN (15 μM) for 12 hours to show the puncta of STING in the ER and detect various proteins in the Triton X-100 insoluble fractions (TI), unless specifically defined. **A** cGAS was knocked out in cells, or cells were co-treated with G140 (30 μM), and stained with STING antibody. STING puncta were observed under confocal microscope (left). The percentage of cells with STING puncta was quantified (right, mean ± s.e.m., n = 3 repeats). **B** Living cells were treated with DHN, the puncta of STING and ER were shown. **C-D** Observation of STING-associated ER structure using electron microscopy. A375 cells (**C**) or STING-APEX-expressing A375 cells (**D**) were treated with DHN for 12 hours, the ER morphology and the location of STING in ER was observed. **E** Indication of STING-associated organelles. Cells were transfected with STING-HA first, the STING-associated organelles were immunoprecipitated and then indicated by various antibodies as indicated (CALR: ER marker; GM130: Golgi marker; Tom20: mitochondria marker; LDHA: Cytosol marker). **F** Cells were treated with DHN, the puncta of STING and GSDME or caspase8 were shown. **G** The CypD-knockdown (left), STING-knockdown (right) or cGAS-knockout (middle) cells were treated with DHN. The localization of STING, cleaved-CASP8, and GSDME in the TI was indicated. **H** Cells were transfected with GFP-V5-turboID or STING-V5-turboID and then labeled with biotin (100 μM) for 10 min, the biotin-labeled proteins were isolated and indicated by corresponding antibodies. Statistical data are presented as mean ± s.e.m. of (n = 3) three independent experiments. Statistical analyses were determined by two-way ANOVA with Tukey's multiple comparisons test (**A**). P values are indicated. All western blots were repeated at least twice and one of them is shown.

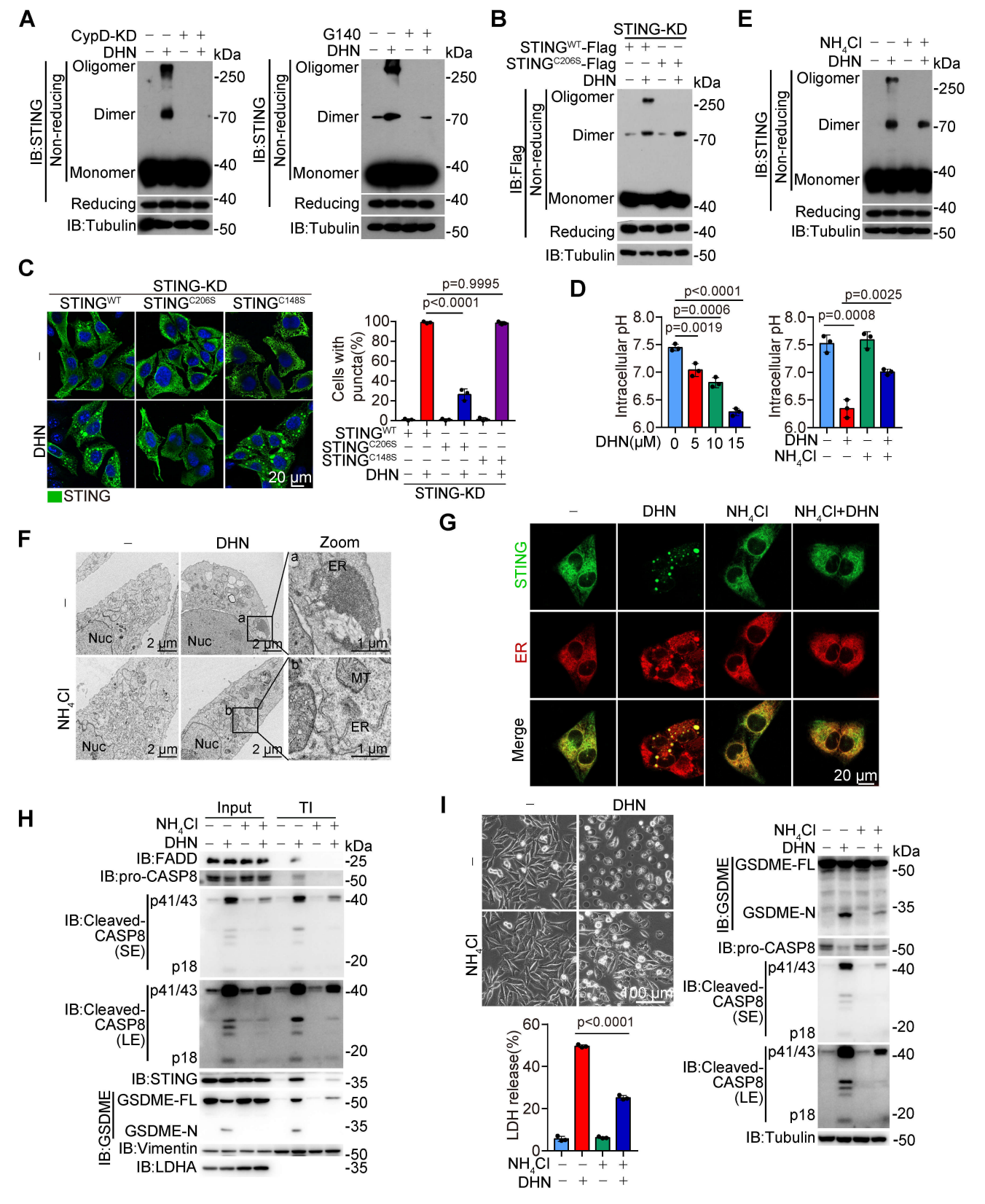
A
CypD-KD
DHN
kDa
IB:STING
Non-reducing
Oligomer
Dimer
Monomer
Reducing
IB:Tubulin
-250
-70
-40
-50
G140
B
STING-KD
STINGWT-Flag
STINGC206S-Flag
IB:Flag
E
NH4Cl
C
STINGWT
STINGC206S
STINGC148S
20 μm
STING
Cells with puncta(%)
p=0.9995
p<0.0001
D
Intracellular pH
p<0.0001
p=0.0006
p=0.0019
DHN(μM) 0 5 10 15
p=0.0025
p=0.0008
F
Zoom
Nuc
2 μm
1 μm
ER
MT
G
STING
ER
Merge
H
Input
TI
IB:FADD
IB:pro-CASP8
IB:Cleaved-CASP8 (SE)
IB:Cleaved-CASP8 (LE)
p41/43
p18
IB:STING
IB:GSDME
GSDME-FL
GSDME-N
IB:Vimentin
IB:LDHA
I
400 μm
LDH release(%)
IB:Tubulin

Fig. 5 DHN-caused ER acid environment promotes the formation of STING aggregates. Melanoma A375 cells were treated with DHN (15 μM) for 12 hours to show the puncta of STING in the ER and detect STING polymer and location of various proteins in TI, for 20 hours to assess pyroptotic features, unless specifically defined. **A** CypD was knocked down in cells (**A**, left), or cells were co-treated with G140 (**A**, right, 30 μM), then polymer of STING was indicated. **B-C** $STING^{WT}$, $STING^{C206S}$ and $STING^{C148S}$ were separately transfected into STING-knockdown cells, then polymer of STING was indicated (**B**). STING puncta were observed under confocal microscope (**C**, left) and the percentage of cells with STING puncta was quantified (**C**, right). **D** Cells were treated with DHN at different concentrations (left), or were co-treated with NH_4Cl (right, 5 mM), followed by measurement of cytosolic pH values. **E-I** Cells were co-treated with NH_4Cl (5 mM), followed by the detections of polymer of STING (**E**), ER morphology using electron microscope (**F**), STING and ER puncta using confocal microscope (**G**), the localization of STING, cleaved-CASP8, and GSDME in the TI (**H**) and pyroptosis (**I**). Tubulin was used to determine the amount of loading proteins. Statistical data are presented as mean ± s.e.m. of (n = 3) three independent experiments. Statistical analyses were determined by one-way ANOVA with Tukey's multiple comparisons test (**D** (left)) and two-way ANOVA with Tukey's multiple comparisons test (**C**, **D** (right), **I**). P values are indicated. All western blots were repeated at least twice and one of them is shown.

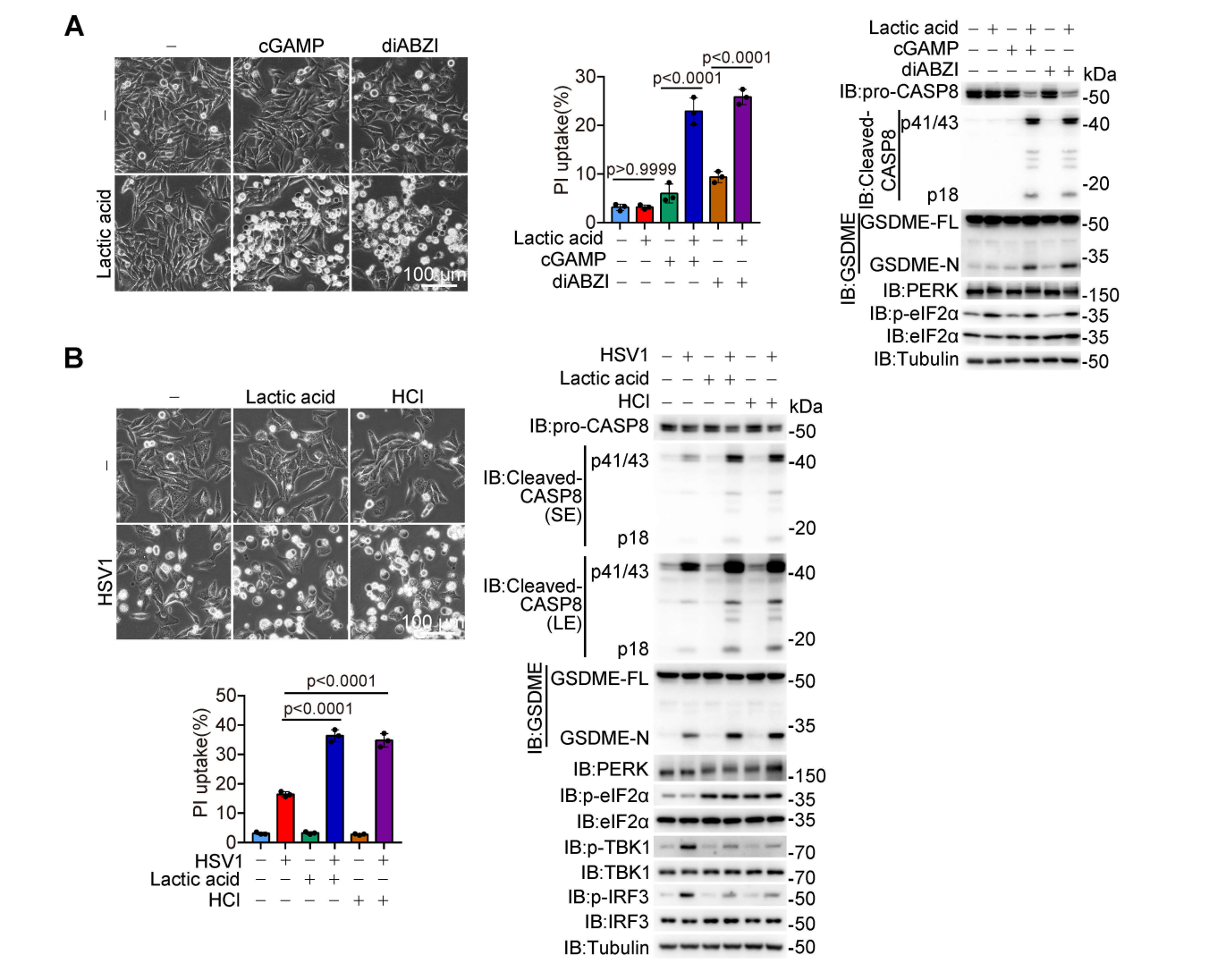
A
–
cGAMP
diABZI
–
Lactic acid
100 μm
PI uptake(%)
p<0.0001
p<0.0001
p>0.9999
Lactic acid – + – + – +
cGAMP – – + + – –
diABZI – – – – + +
Lactic acid – + – + – +
cGAMP – – + + – –
diABZI – – – – + +
kDa
IB:pro-CASP8
-50
IB:Cleaved-CASP8
p41/43
-40
p18
-20
IB:GSDME
GSDME-FL
-50
GSDME-N
-35
IB:PERK
-150
IB:p-eIF2α
-35
IB:eIF2α
-35
IB:Tubulin
-50
B
–
Lactic acid
HCl
HSV1
100 μm
PI uptake(%)
p<0.0001
p<0.0001
HSV1 – + – + – +
Lactic acid – – + + – –
HCl – – – – + +
HSV1 – + – + – +
Lactic acid – – + + – –
HCl – – – – + +
kDa
IB:pro-CASP8
-50
IB:Cleaved-CASP8 (SE)
p41/43
-40
p18
-20
IB:Cleaved-CASP8 (LE)
p41/43
-40
p18
-20
IB:GSDME
GSDME-FL
-50
GSDME-N
-35
IB:PERK
-150
IB:p-eIF2α
-35
IB:eIF2α
-35
IB:p-TBK1
-70
IB:TBK1
-70
IB:p-IRF3
-50
IB:IRF3
-50
IB:Tubulin
-50

Fig. 6 cGAS activation converges with intracellular acidification to induce pyroptosis. Melanoma A375 cells were treated with different stimulants for 20 hours to assess pyroptotic features (including characteristic morphology, caspase8/GSDME cleavage, and LDH release), unless specifically defined. **A** Cells were co-treated of lactic acid (20 mM) and 2,3'-GAMP (10 μg/ml) or diABZI (10 μM), followed by the detection of pyroptosis. **B** Cells were infected with HSV1 (10 moi) and in the presence of lactic acid (20 mM) or HCl (20 mM), followed by the detection of pyroptosis. Tubulin was used to determine the amount of loading proteins. Statistical data are presented as mean ± s.e.m. of (n = 3) three independent experiments. Statistical analyses were determined by two-way ANOVA with Tukey's multiple comparisons test (**A**, **B**). P values are indicated. All western blots were repeated at least twice and one of them is shown.

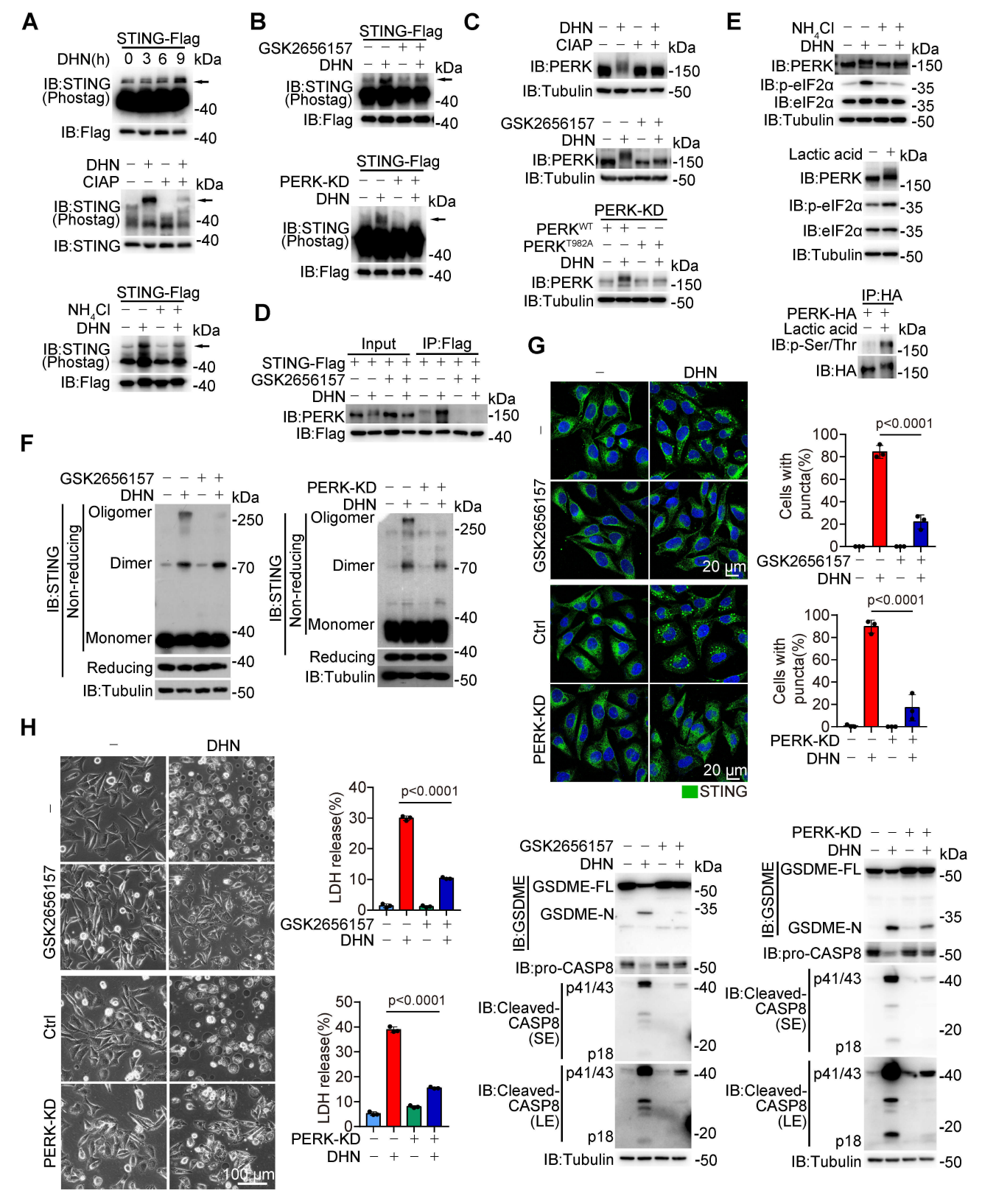
A
STING-Flag
DHN(h) 0 3 6 9 kDa
IB:STING (Phostag)
IB:Flag
DHN
CIAP
IB:STING
NH4Cl
B
GSK2656157
PERK-KD
C
IB:PERK
IB:Tubulin
PERKWT
PERKT982A
D
Input
IP:Flag
E
IB:p-eIF2α
IB:eIF2α
Lactic acid
IP:HA
PERK-HA
IB:p-Ser/Thr
IB:HA
F
Oligomer
Dimer
Monomer
Reducing
Non-reducing
G
STING
Ctrl
20 μm
p<0.0001
Cells with puncta(%)
H
LDH release(%)
100 μm
IB:GSDME
GSDME-FL
GSDME-N
IB:pro-CASP8
IB:Cleaved-CASP8 (SE)
IB:Cleaved-CASP8 (LE)
p41/43
p18

Fig.7 DHN-induced phosphorylation of STING by PERK facilitates the polymerization of STING. Melanoma A375 cells were treated with DHN (15 μM) for 12 h to detect STING phosphorylation, the puncta of STING in the ER, and STING polymer and location of various proteins in TI, for 20 h to assess pyroptotic features, unless specifically defined. **A-B** Control (**A**, top) or PERK knockdown A375 cells (**B**, bottom) were treated with DHN in the presence of NH_4Cl (**A**, bottom, 5 mM) or GSK2656157 (**B**, top, 10 μM). Cell lysates were incubated with CIAP (**A**, middle). STING phosphorylation was analyzed using Phos-tag assays. **C** Cell lysates were incubated with CIAP (top). Cells were co-treated with GSK2656157 (middle, 10 μM), and $PERK^{WT}$ or $PERK^{T982A}$ were separately transfected into PERK-knockdown cells (bottom). **D** Cells were co-treated with GSK2656157 (10 μM), the interaction between STING and PERK was determined. **E** Cells were co-treated with NH_4Cl (top, 5 mM) and DHN, or treated with lactic acid (middle and bottom, 20 mM), followed by the detection of PERK and eIF2α phosphorylation. **F-H** Cells were co-treated with GSK2656157 (10 μM), or subjected to PERK knockdown, followed by the detections of STING polymerization (**F**), STING puncta (**G**) and pyroptosis (**H**). Tubulin was used to determine the amount of loading proteins. Statistical data are presented as mean ± s.e.m. of (n = 3) three independent experiments. Statistical analyses were determined by two-way ANOVA with Tukey's multiple comparisons test (**G**, **H**). P values are indicated. All western blots were repeated at least twice and one of them is shown.

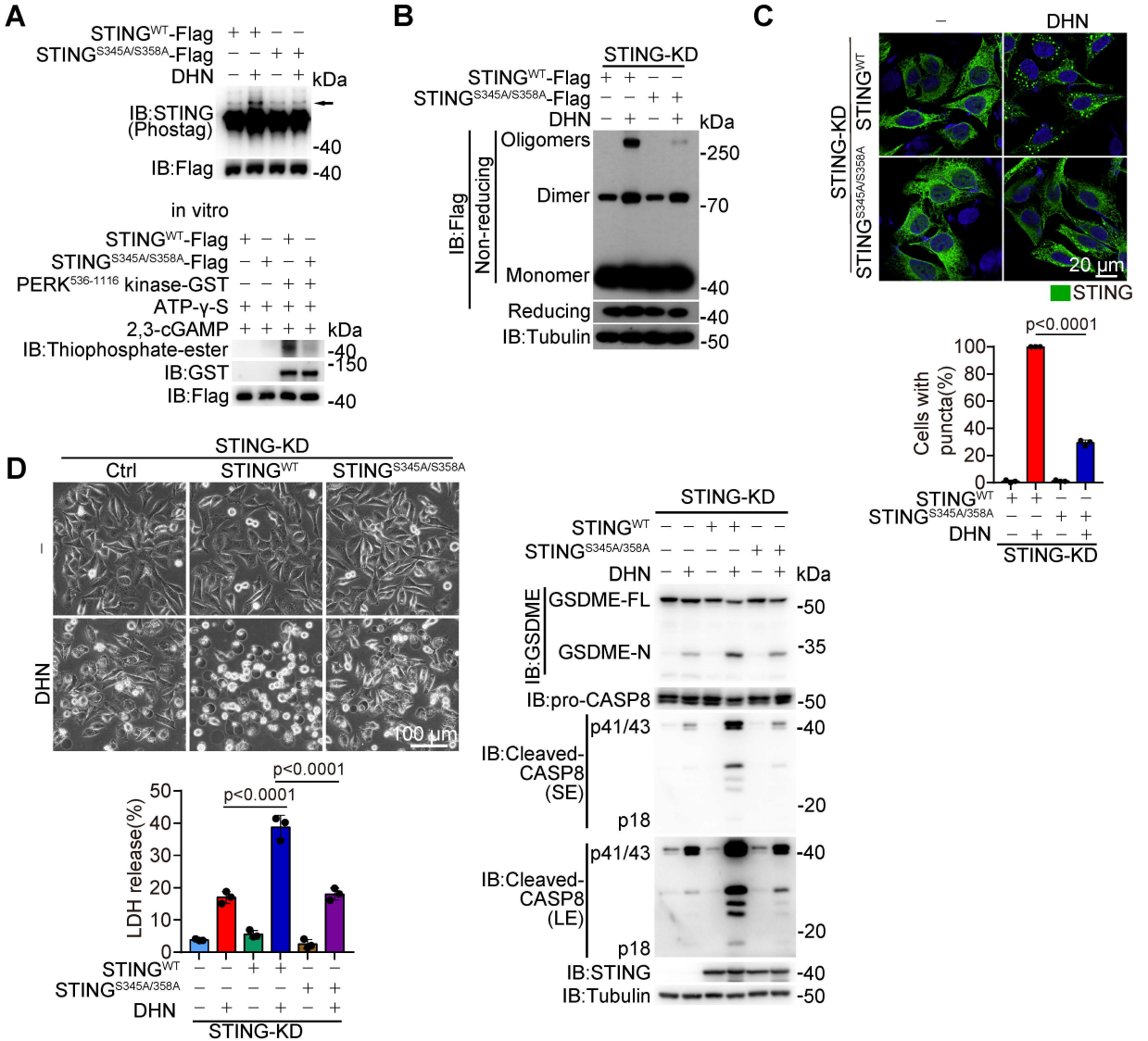
A
STINGWT-Flag
STINGS345A/S358A-Flag
DHN
kDa
IB:STING (Phostag)
IB:Flag
-40
in vitro
PERK536-1116 kinase-GST
ATP-γ-S
2,3-cGAMP
IB:Thiophosphate-ester
IB:GST
-150
B
STING-KD
Oligomers
Dimer
Monomer
Non-reducing
IB:Flag
-250
-70
Reducing
IB:Tubulin
-50
C
DHN
STING-KD
20 μm
STING
p<0.0001
Cells with puncta(%)
D
Ctrl
100 μm
LDH release(%)
IB:GSDME
GSDME-FL
GSDME-N
-35
IB:pro-CASP8
IB:Cleaved-CASP8 (SE)
IB:Cleaved-CASP8 (LE)
p41/43
p18
-20
IB:STING

Fig.8 Phosphorylation of STING at Ser345 and Ser358 by PERK is critical for DHN-induced pyroptosis. Melanoma A375 cells were treated with DHN (15 μM) for 12 h to detect STING phosphorylation, the puncta of STING in the ER, for 20 h to assess pyroptotic features, unless specifically defined. **A** $STING^{WT}$ and $STING^{S345A/S358A}$ were transfected into STING-knockdown cells, followed by the detection of STING phosphorylation (top). $STING^{WT}$ and $STING^{S345A/S358A}$ was incubated with PERK *in vitro* (bottom). **B-D** $STING^{WT}$ and $STING^{S345A/S358A}$ were transfected into STING-knockdown cells, followed by the detections of STING polymerization (**B**), STING puncta (**C**) and pyroptosis (**D**). Tubulin was used to determine the amount of loading proteins. Statistical data are presented as mean ± s.e.m. of (n = 3) three independent experiments. Statistical analyses were determined by two-way ANOVA with Tukey's multiple comparisons test (**C**, **D**). P values are indicated. All western blots were repeated at least twice and one of them is shown.

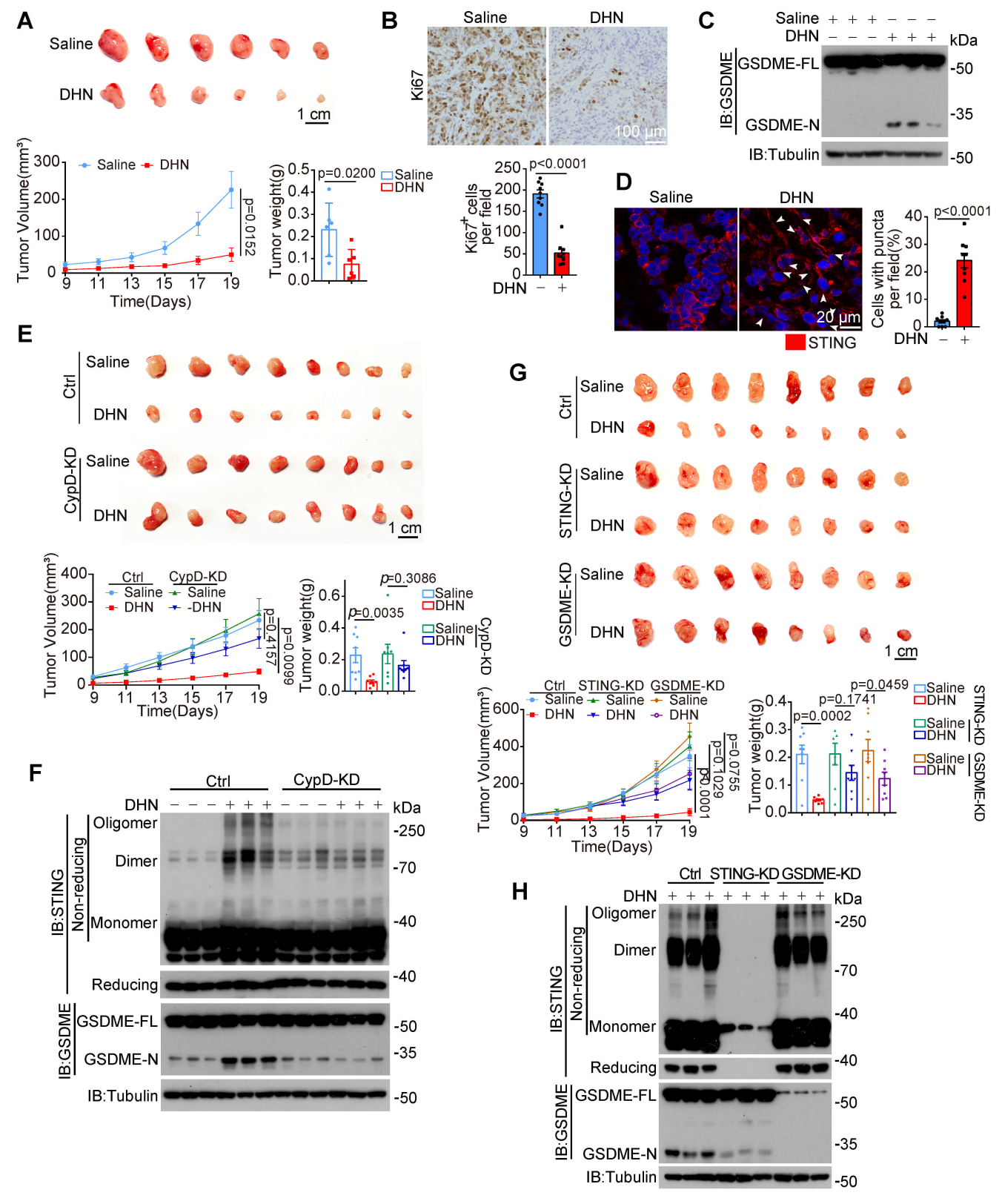
A
Saline
DHN
1 cm
Tumor Volume(mm³)
Saline
DHN
p=0.0152
Time(Days)
Tumor weight(g)
p=0.0200
B
Saline
DHN
Ki67
100 μm
Ki67+ cells per field
p<0.0001
C
Saline
DHN
kDa
IB:GSDME
GSDME-FL
GSDME-N
IB:Tubulin
-50
-35
-50
D
Saline
DHN
20 μm
STING
Cells with puncta per field(%)
p<0.0001
E
Ctrl
CypD-KD
Saline
DHN
1 cm
Tumor Volume(mm³)
p=0.4157
p=0.0099
Tumor weight(g)
p=0.3086
p=0.0035
F
Ctrl
CypD-KD
DHN
kDa
IB:STING
Non-reducing
Oligomer
Dimer
Monomer
Reducing
IB:GSDME
GSDME-FL
GSDME-N
IB:Tubulin
-250
-70
-40
-40
-50
-35
-50
G
Ctrl
STING-KD
GSDME-KD
Saline
DHN
1 cm
Tumor Volume(mm³)
p=0.0755
p=0.1029
p<0.0001
Time(Days)
Tumor weight(g)
p=0.0459
p=0.1741
p=0.0002
H
Ctrl
STING-KD
GSDME-KD
DHN
kDa
IB:STING
Non-reducing
Oligomer
Dimer
Monomer
Reducing
IB:GSDME
GSDME-FL
GSDME-N
IB:Tubulin
-250
-70
-40
-40
-50
-35
-50

Fig.9 DHN inhibits tumor growth by inducing pyroptosis in mice. A375 cells (2×10^6) were injected subcutaneously into the posterior flanks of nude mice. After four days, DHN was intraperitoneally administered to the mice every other day for 2 weeks. The tumor volume and weight were recorded at the indicated times. **A-D** A375 cells were injected into BALB/c-nu mice to form subcutaneous xenografts (**A**, n = 6). The expression of Ki67 is shown (**B**; n = 9 fields from three independent tumor tissues). Tumors were collected for detection of GSDME (**C**). STING puncta were indicated by white arrows (**D**, left) and the percentage of cells with STING puncta was quantified (**D**, right; n = 9 fields from three independent tumor tissues). **E-H** A375 cells with or without knockdown of CypD (**E, F**), STING or GSDME (**G, H**) were injected into BALB/c-nu mice to form subcutaneous xenografts (n = 8). Tumors were collected for detection of GSDME and monomer, dimer and oligomers of STING. Tubulin was used to determine the amount of loading proteins. Statistical analyses were determined by unpaired two-tailed Student's t-test (**A**, **B**, **D**) and two-way ANOVA with Tukey's multiple comparisons test (**E**, **G**). P values are indicated.

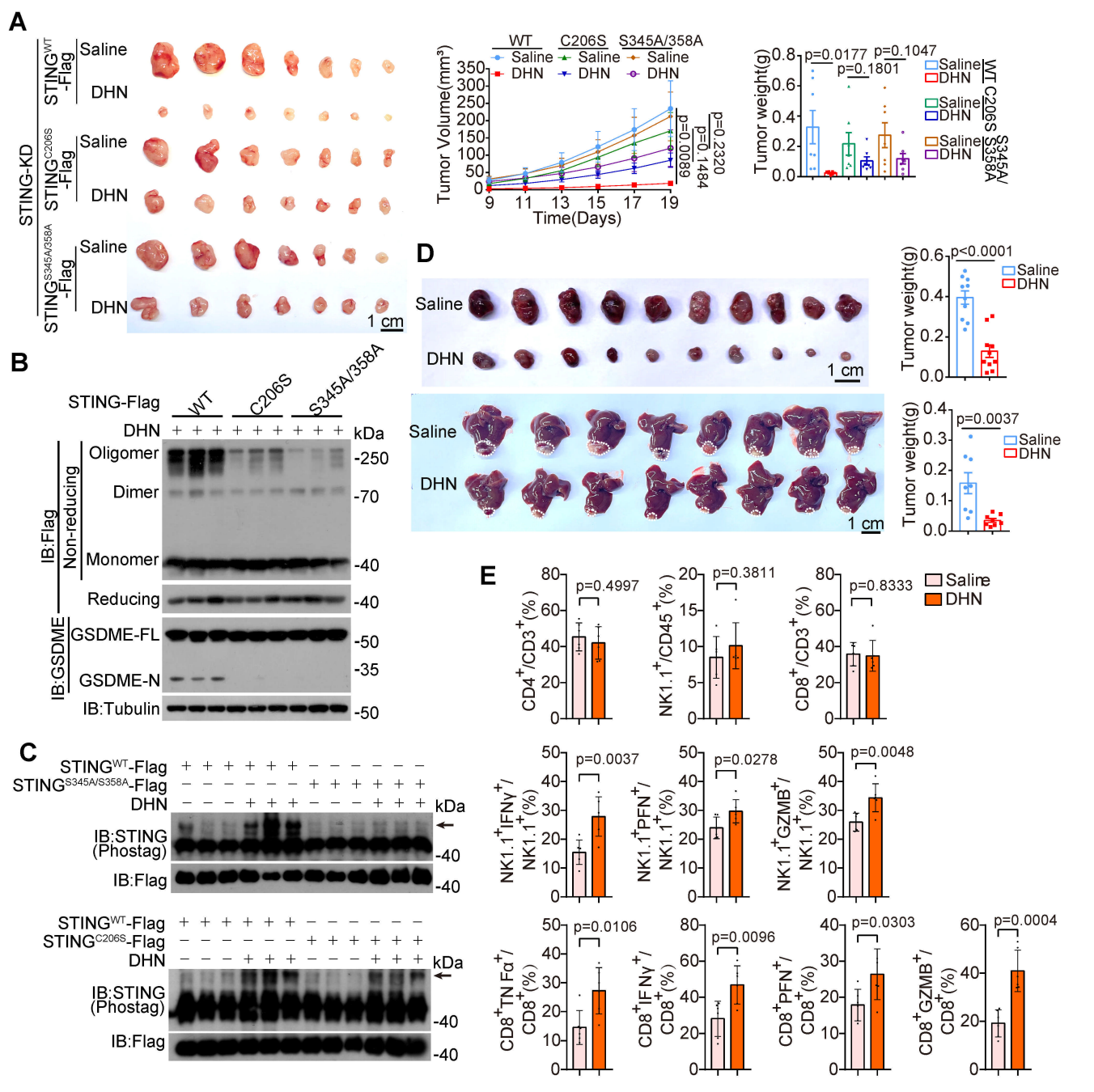
A
STING-KD
STING^WT-Flag
STING^C206S-Flag
STING^S345A/358A-Flag
Saline
DHN
1 cm
WT
C206S
S345A/358A
Tumor Volume(mm³)
Time(Days)
p=0.0089
p=0.1484
p=0.2320
Tumor weight(g)
p=0.0177
p=0.1801
p=0.1047
B
STING-Flag
DHN
kDa
Oligomer
Dimer
Monomer
Reducing
GSDME-FL
GSDME-N
IB:Tubulin
IB:Flag
Non-reducing
IB:GSDME
-250
-70
-40
-50
-35
C
STING^WT-Flag
STING^S345A/S358A-Flag
STING^C206S-Flag
IB:STING (Phostag)
IB:Flag
D
p<0.0001
p=0.0037
E
CD4+/CD3+(%)
NK1.1+/CD45+(%)
CD8+/CD3+(%)
p=0.4997
p=0.3811
p=0.8333
NK1.1+IFNγ+/NK1.1+(%)
NK1.1+PFN+/NK1.1+(%)
NK1.1+GZMB+/NK1.1+(%)
p=0.0037
p=0.0278
p=0.0048
CD8+TNFα+/CD8+(%)
CD8+IFNγ+/CD8+(%)
CD8+PFN+/CD8+(%)
CD8+GZMB+/CD8+(%)
p=0.0106
p=0.0096
p=0.0303
p=0.0004

Fig.10 DHN induces anti-tumor immune responses in mice tumor model. A375 cells (2×10^6) were injected subcutaneously into the posterior flanks of nude mice. After four days, DHN was intraperitoneally administered to the mice every other day for 2 weeks. The tumor volume and weight were recorded at the indicated times. **A-C** A375 STING-knockdown cells with expression of $STING^{WT}$, $STING^{C206S}$ or $STING^{S345A/358A}$ were injected into BALB/c-nu mice to form subcutaneous xenografts (**I**, n = 7). Tumors were collected for detection of GSDME (**A**), monomer, dimer and oligomers of STING (**B**) and STING phosphorylation (**C**). **D** B16 (top, n = 10) or Hepa1-6 (bottom, n = 8) cells were injected into C57/BL6 mice to form xenografts. DHN was intraperitoneally administered to the mice. **E** B16 cell-derived xenograft tumors were collected 24 h after DHN (10 mg/kg) administration and then analysed using flow cytometry to determine the proportion and activation status of immune cells within the tumor microenvironment (n = 5). Tubulin was used to determine the amount of loading proteins. Statistical analyses were determined by unpaired two-tailed Student's t-test (**D**, **E**) and two-way ANOVA with Tukey's multiple comparisons test (**A**). P values are indicated.